

Revisiting Audio Pattern Recognition for Asthma Medication Adherence: Evaluation with the RDA Benchmark Suite

Nikos D. Fakotakis, Stavros Nousias, Gerasimos Arvanitis, Evangelia I. Zacharaki, Konstantinos Moustakas

*Department of Electrical and Computer Engineering, University of Patras, Greece

Abstract—Asthma is a common, usually long-term respiratory disease with negative impact on society and the economy worldwide. Treatment involves using medical devices (inhalers) that distribute medication to the airways, and its efficiency depends on the precision of the inhalation technique. Health monitoring systems equipped with sensors and embedded with sound signal detection enable the recognition of drug actuation and could be powerful tools for reliable audio content analysis. This paper revisits audio pattern recognition and machine learning techniques for asthma medication adherence assessment and presents the *Respiratory and Drug Actuation (RDA) Suite*¹ for benchmarking and further research. The RDA Suite includes a set of tools for audio processing, feature extraction and classification and is provided along with a dataset consisting of respiratory and drug actuation sounds. The classification models in RDA are implemented based on conventional and advanced machine learning and deep network architectures. This study provides a comparative evaluation of the implemented approaches, examines potential improvements and discusses challenges and future tendencies.

Index Terms—Asthma, Feature extraction, Inhaler medication adherence, Machine learning, Respiratory sounds

I. INTRODUCTION

ASTHMA is a chronic inflammatory condition of the airways, with over 235 million people [1]–[3] suffering worldwide. The direct cost associated with asthma has risen a significant burden on society and healthcare systems [4], [5]. Asthma is a common disease among children and one of the most common chronic conditions. It is characterized by recurrent attacks of wheezing, breathlessness, dyspnea, chest tightness and coughing, known as asthma attacks [6]. It deteriorates the quality of life for patients and their families up to a level, leading to increased healthcare cost, poor clinical outcomes and increased morbidity rates [7]. The variety of obstructive respiratory diseases [8], [9] reveals the importance for innovative models that could help patients face their unpleasant condition and enjoy a better quality of life [10]. There is evidence that adherence to asthma treatment is variable, hindering the proper management of the disease [11]. Detailed constructive feedback from clinicians on inhaler usage may motivate patients to focus more on treatment adherence, which in turn may improve their quality of life, prevent exacerbation and hospitalization and, eventually, reduce mortality rates associated with chronic respiratory diseases [12].

Inhaled aerosol therapies are the main treatment of obstructive lung diseases [13]. Inhaler based monitoring devices were introduced at the beginning of the 1980s and, since then, have been developed, mainly for the proper assessment of medication adherence. These devices are presented in section II. Aerosol devices deliver a fixed medication dose, rapidly and directly into the airways, from a pressurized canister, containing a medication/propellant mixture [14], [15]. The efficient and effective management of asthma is strongly connected with the patient adherence to the prescribed action plan, while reduced adherence has been strongly linked with significant indicators of health degradation. Active feedback may encourage patients to improve their adherence and manage their condition better. For this purpose, specialists have developed methodologies to monitor inhaler users and understand if patients use their inhaler devices with the appropriate technique and at the correct time duration. Audio process phenomenology requires the transformation of the measured data to extract the desired information (section IV). The current methods exploit machine learning and, mainly, deep learning approaches to develop classification models that, given as input the monitored acoustic signals, automatically recognize the phase of respiration and detect the drug inhalation onset (section V). Often, time-frequency analysis of the respiratory signals [16]–[18] is performed prior to classification in order to extract a variety of features, critical for extensive analysis. Acoustic analysis of breathing has been employed to detect the different phases of respiration, such as inhalation, exhalation, and drug actuation [19]–[21]. Many of these works are related to personalized management services on obstructive respiratory diseases, aiming to provide methodologies for medication adherence monitoring [22]. Specifically, these studies either focus on device-integrated solutions, using pressure-activated switches [23], [24] or on ambient sound analysis, intelligent systems [25]. Despite their coalescent differences, every approach targets the detection of drug actuation and recognition of respiratory events for the right drug assessment and procedure management.

Audio processing problems can lead to some complex and intricate approaches, in order to perform pattern extraction of critical information, especially on noisy or sometimes incomplete sound measurements [26], [27]. Signal processing techniques can effectively extract useful information. However, they can be pretty difficult to develop. The adherence of patients to their medication intake, in terms of prescribed

¹<https://gitlab.com/vvr/monitoring-medication-adherence/rda-benchmark>

dosage and careful usage of inhaler devices, is critical for controlling the disease. 24% of asthma exacerbation and 60% of hospitalization are caused by poor medication adherence [28]. Studies suggest that up to 67% of clinicians cannot describe the steps correctly or demonstrate correct inhaler usage, so we focus on the optimization of adherence and the management of non-adherence, through the use of systems, with methodologies that consider patient preferences, in treatment and care decisions [29], [30]. For the experiments, it was used a pressurized metered-dose inhaler (pMDI), where patients were instructed to actuate the canister of the pMDI as they begin a "slow" and "deep" inhalation [31]. In order to ensure that the medication reaches the lower airways, the inhalation in drug actuation must be steadily below 90 L/min [32], [33]. Because the majority of patients perform at least one step of the inhalation technique incorrectly (insufficient respiratory effort), systematic training is required to achieve optimal inhaler technique [34]. Through breathing, inhalation and exhalation, the respiratory system facilitates the exchange of gases between the air and the blood and between the blood and the body's cells [35]. Modern signal analysis techniques have been applied to extract features from inhalation sounds that characterize events, such as drug actuation sounds or respiratory flow rate. Hence, we hypothesized that by analyzing the acoustics of inhalation, in a group of patients with a variety of respiratory and non-respiratory diseases, we could assess the accuracy, sensitivity and specificity of the state of the art methods on inhalation sounds' classification [36].

This paper presents an extensive review and discussion on the state-of-the-art methods and tools for acoustic analysis, and content-based audio classification of inhaler sounds on medication adherence, which could be used to improve techniques on aerosol therapy [37]. The rest of the paper is organized as follows: Section II provides a synopsis on the state of the art of inhaler devices with different system designs. Section III presents the annotation on RDA dataset recordings after the feature extraction procedure, which is constituted in section IV and has been used on different approaches and the methodological aspects for audio recordings. Section V analyzes the different frameworks and architectural components and the methodological aspects, that are used for the detection and recognition of respiratory and actuation sounds from RDA dataset. Section VI describes the experimental evaluation of each structure and their accuracy comparisons, while section VII gives recommendations for future directions on acoustic analysis of inhaler sounds, in the field of machine learning and, finally, section VIII concludes this study.

II. INHALER TECHNIQUE MONITORING SYSTEMS

There has been an increasing interest from researchers and software architects for medication adherence monitoring devices. The first inhalation device used for asthma was the pressurized metered-dose inhaler in the 1950s. Today, there are many devices available with different techniques to support the proper drug intake [38]. We briefly present representative technologies utilized over time:

- SmartMist™ is a microprocessor-controlled device, widely used in academic research that optimizes drug deposition in the lung, emitted from metered-dose inhalers (MDIs) [39]–[41].
- Diskus Adherence Logger (DAL) is an inhaler device with a small size sensor, designed to recognize the motion of the dose delivery level in Diskus DPIs and to communicate with the event recorder chip, for control and data uploading to a computer [42], [43].
- The SmartTrack is an innovative adherence monitoring device, for pressurized metered-dose inhalers that consist of an LCD screen and four push buttons that allow the navigation in the device menu [44], [45].
- The SmartTurbo (Adherium (NZ) Ltd, Auckland, New Zealand) is an electronic monitor that combines its use with a Turbuhaler device (AstraZeneca, UK) and consists of electromechanical sensors to identify the state on the mouthpiece of the inhaler [46]–[48].
- The Asthmapolis system relies on technology that monitors the location of blister actuations, allowing the user to gain information about the disease, such as date and time of the usage [49] and to collect timely and geographically specific information about asthma management, with a clear picture of health status [50], [51].
- The Inspiromatic™ is an innovative approach to inhaler enhancement, based on the real-time inhalation flow measurements [53].
- Sensohaler is a novel device that incorporates MDIs, with fundamental acoustic sensing functionalities that are used for the prediction of volumetric flow rate [54].
- The T-Haler device is based on another innovative approach for the design of a MDI, with enhanced monitoring key performance characteristics, [53].
- Furthermore, an integrated system was presented in [55], consisting of three main parts, the monitoring device, the smartphone application and the cloud processing server part.

III. EVALUATION DATASET

The central aim of this research is to identify associations between high-level classification labels and low-level features extracted from audio clips of different semantic activities. We investigate the clinical applicability of different audio-based signal processing methods for assessing medication adherence. The dataset consists of recordings acquired in an acoustically controlled setting, free of ambient indoor environment noise, at the University of Patras. Three subjects, who were familiar with the inhaler technique, participated in the study. The participants were instructed to use the inhaler, as typically performed in a clinical procedure. For each and every participant informed consent was obtained. During breathing and drug actuation, the audio signals were acquired by a microphone attached to the inhalation device, communicating with a mobile phone via Bluetooth. The addition of the adherence monitoring device did not impact the normal functioning of the inhaler, which had a full placebo canister. In total, 370 audio files

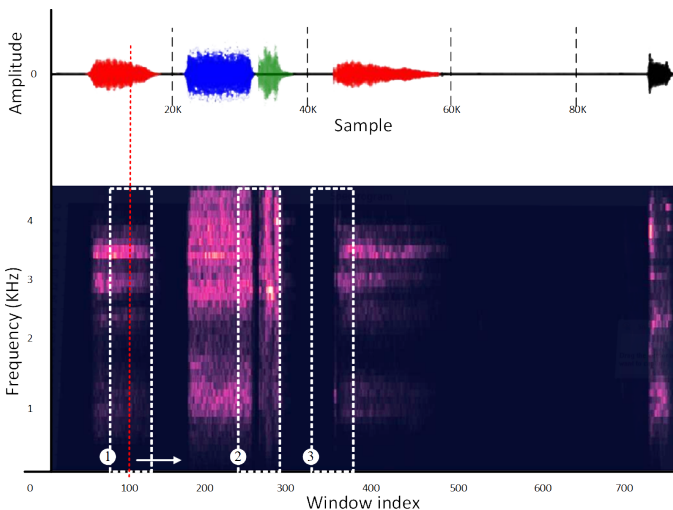


Fig. 1: Audio timeseries colored with ground truth labels (top) and visualization of the corresponding spectrogram, within a sliding window (bottom). Events include inhalation (blue), drug actuation (green), exhalation (red) and environmental noise (black). Window sliding positions might include non-mixed states (window 1) or transitional states, e.g. from inhalation to drug actuation (window 2) and breath holding to exhalation (window 3), respectively. The class label of the sliding windows corresponds to the central point. Reproduced with permission from Pettas et al. [52]

were recorded with a different duration each, containing an entire inhaler use case, with respiratory flow ranging on 180-240 L/min. Each audio recording was sampled with a 8KHz sampling frequency, as a mono channel WAV file, at 8-bit depth. The audio recordings were segmented and annotated by a human specialist into inhaler actuation, exhalation, inhalation and environmental noise. The obtained segments (of non-mixed states) were of variable length and, for some methods, were further segmented into frames of fixed length for the purposes of feature extraction, as described in section IV. The acoustic signal of a typical patient recording is shown in Figure 1. The constructed database overall consisted of 193 drug actuation segments, 319 inhalation and 620 exhalation segments and 505 noise segments, ready to be used for audio sound recognition using different sets of features.

IV. PRELIMINARIES ON FEATURE EXTRACTION AND AUDIO DESCRIPTORS

Various features have been extracted from audio signals, both in temporal and spectral domain, and have been used as a basis for audio analysis algorithms [56]. It is typical for audio analysis to extract the features across sliding time windows, in order to capture the class or activity within that particular moment in time. The extraction and selection of robust and descriptive features for specific applications is the main challenge in designing audio classification systems [57], [58]. We have elaborated our work on the characterization of the audio signals, using several spectral features and audio patterns, as proposed in the literature. We first denote a signal

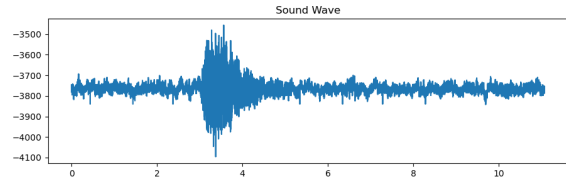


Fig. 2: Sound wave plot of the first inhalation recording.

as a time series, $x(t), t = 1, \dots, T$, in the time domain. As the signal is changing through time, it is assumed that on short time scales is statistically stationary and thus, statistical features can be extracted through a windowing process, in which the signal is segmented into small, possibly overlapping, time windows (frames) of the same length (N). We denote as $x_n(i)$ the i^{th} sample in the n^{th} frame audio signal, where $i = 1, \dots, N$.

A. Volume in time domain analysis

Volume in the time domain, is a reliable indicator for silence detection. Therefore, it can segment audio sequences and determine clip boundaries. It is commonly perceived as loudness since natural sounds are pressure waves, with different amounts of power that modifies them and different distribution for each audio recording. In electronic sounds, the physical quantity is amplitude, and therefore volume is often calculated as the Root-Mean-Square (RMS) of amplitude. Volume of the n^{th} frame is calculated by the following formula:

$$V(n) = \sqrt{1/N} \sum_{i=1}^N x_n^2(i) \quad (1)$$

where $V(n)$ is the volume. Figure 2 shows the volume of the first recording.

B. Zero Crossing Rate analysis

Zero-Crossing Rate (ZCR) is defined formally as the number of time-domain zero-crossings, within a defined region of signal, divided by the number of samples of that region [59]: in the context of discrete-time signals, a zero crossing is said to occur if successive samples have different algebraic signs. The zero-crossing finds the rate at which the signal changes from positive to negative and vice-versa [60], [61]. In some cases, only the "positive-going" or "negative-going" crossings are counted, rather than all the crossings, since, logically, between a pair of adjacent positive zero-crossings, there must be one negative zero-crossing [62]. This feature has been used extensively in speech recognition and music information retrieval to classify percussive sounds.

$$ZCR = \frac{1}{T-1} \sum_{t=1}^{T-1} J\{x(t)x(t-1) < 0\}$$

where $x(t)$ is a time domain signal of length T and $J\{y\}$ is a logical function returning one, if its argument is true and zero, otherwise [63].

C. Spectrogram analysis

Any sound signal can be expressed in the frequency spectrum, which shows the average amplitude of various frequency components in the audio signal and the frequency distribution. To obtain frequency domain features, the spectrogram of an audio clip in the form of Short-Time Fourier Transform (STFT) is calculated for each audio frame. The spectrogram is used for the extraction of two features, namely frequency centroid and frequency bandwidth.

D. Cepstrum analysis

The first paper on cepstrum analysis [64] defined the cepstrum as "the power spectrum of the logarithm of the power spectrum". The cepstrum results from the Inverse Discrete Fourier Transform (IDFT) of a signal's log magnitude of the Discrete Fourier Transform (DFT). It has been used in speech analysis for determining voice pitch (by accurately measuring the harmonic spacing), but also for separating the formants (transfer function of the vocal tract) from voiced, and unvoiced sources, which led quite early to similar applications in mechanics [65]. The definition of the complex cepstrum is:

$$C_c(\tau) = \mathcal{F}^{-1} \left\{ \log(F(f)) \right\} = \mathcal{F}^{-1} \left\{ \ln(A(f)) + j\phi(f) \right\} \quad (2)$$

where \mathcal{F}^{-1} is the IDFT and F is the DFT, in terms of the amplitude and phase of the spectrum [66].

E. Mel Frequency Cepstral Coefficients Analysis and Power Spectral Density

Audio feature extraction is used to decrease the dimensionality of the input vector while maintaining the discriminating power of the signal. It is an important part to prepare data for the sound identification process, and this kind of analysis is derived from the cepstral representation of audio data [67]. A systematic study of various spectral features can be found in (Kinnunen 2004) [68]. The Mel Frequency Cepstral Coefficient (MFCC) feature extraction is a technique in sound recognition that is based on the frequency domain of Mel scale for human ear scale [69]. MFCC's extraction is a significant technique, also, due to efficient computation schemes and its robustness in the presence of different noise [70]. To compute the MFCC's, a Hamming window is multiplied with the overlapping segments after windowing, and the Fast Fourier Transform (FFT) is computed for every frame. The equation for Hamming window sequence can be defined by:

$$w(n) = \alpha - \beta \cos\left(\frac{2\pi n}{N-1}\right) \quad \text{for} \quad -\frac{N-1}{2} \leq n \leq \frac{N-1}{2} \quad (3)$$

with $\alpha = 0.54$ and $\beta = 1 - \alpha = 0.46$. For each frame we take the periodogram-based Power Spectral Density (PSD) estimation:

$$\hat{P}_i(k) = \frac{1}{N} |X_i(k)|^2 \quad (4)$$

where $X_i(k)$ is the complex DFT of the signal $x(n)$, with N samples:

$$X(k) = \sum_{n=\frac{N}{2}-1}^{\frac{N}{2}} x(n) \exp\left(-j2\pi k \frac{n}{N}\right) \quad (5)$$

The power spectral density function helps calculate the total power contained in each spectral component of a specific signal. Power spectrum of any time-domain signal $x(t)$, helps to determine the distribution of the variance of data $x(t)$, over frequency domain, in the form of spectral components, into which the actual signal can be decomposed [71]. This is motivated by the human cochlea (an organ in the ear), which vibrates at different spots, depending on the frequency of the incoming sounds. Depending on location in the cochlea that vibrates, different nerves fire, informing the brain that specific frequencies are present. Therefore, the estimated PSD of the signal is related to the modulus of its DFT [72].

After this step, we continue the calculations, with the spectrum segmented into a number of critical bands employing filterbanks. The filterbank, typically, consists of overlapping triangular filters, which are spaced linearly, in a perceptual Mel scale. Then, we calculate the Mel filterbanks in order to examine how much energy exists in various frequency regions. The Mel scale determines how to space the filterbanks and how wide to make them. It relates the perceived frequency of a pure tone to its actual measured frequency. Once we have the filterbank energies, we compute their logarithm. The logarithm allows us to use cepstral mean subtraction, which is a channel normalization technique. Finally, Discrete Cosine Transformation (DCT) is applied to the logarithm of the filterbank outputs, which results in the raw MFCC vector [73]. Because our filterbanks are all overlapping, the filterbank energies are quite correlated with each other. The DCT decorrelates the energies, so as diagonal covariance matrices can be used to model the features in the various classifiers.

There can be variations on this process, for example, differences in the shape or spacing of the windows used to map the scale [74] or addition of dynamics features, such as "delta" and "delta-delta" (first- and second-order frame-to-frame difference) coefficients. Exponentiating the log Mel-filter bank spectrum before the cepstrum computation, can significantly reduce the sensitivity of the cepstra to spurious low energy perturbations [75]. The difference between the cepstrum and the Mel-frequency cepstrum is that in the MFCC, the frequency bands are equally spaced on the Mel scale, which approximates the human auditory system's response more closely, than the linearly-spaced frequency bands, used in the normal cepstrum. This frequency warping can permit for better representation of sound in audio compression. MFCC's have been successfully used in speech and music applications, playing a central part in recent efforts to complete machine audition [76].

F. Wavelet Transform analysis

The wavelet transform can construct a time-frequency representation of a signal that offers very good time and frequency

localization. The wavelet transform, with the wavelet ψ of a signal $x(t)$ is defined as:

$$W_{\psi}^x(a, b) = \frac{1}{\sqrt{c_{\psi}|a|}} \int_{-\infty}^{\infty} x(t)\psi\left(\frac{t-b}{a}\right) dt \quad (6)$$

where a is called dilatation and b translation parameter. The Morlet wavelet, consisting of a sinusoid multiplied by a Gaussian window, is commonly used, because its scale-frequency relationship requires less computation, as the peak frequency is equal to the center frequency of the wavelet. The Morlet wavelet ψ , which is sometimes called Gabor wavelet, has some impressive mathematical and biological properties and is given by:

$$\psi(t) = \frac{1}{\pi^{\frac{1}{4}}} \left(e^{i2\pi f_0 t} - e^{-(i2\pi f_0)^2/2} \right) e^{-t^2/2} \quad (7)$$

where f_0 is the center frequency of the mother wavelet [77].

1) *Continuous Wavelet Transform*: In definition, the Continuous Wavelet Transform (CWT) is a convolution of the input data sequence, with a set of functions generated by the mother wavelet. It provides an over-complete representation of a signal by letting the translation and scale parameter of the wavelets vary continuously [78], [79]. The convolution can be calculated in the time-domain or in the frequency-domain, by using an FFT algorithm.

For the STFT, a fixed width segment size controls the time-frequency resolution trade-off. This results in a single resolution in time and a single resolution in frequency, regardless of the rendered frequency. In contrast, wavelet analysis is a multi-resolution method. The time-frequency resolution is not constant but varies with frequency. Multi-resolution analysis was designed for the common condition, where high-frequency components exist for a short duration within a signal and low-frequency components are more persistent. Short-lived high frequency components need strong time localization. In order to achieve this, the frequency resolution of high frequency components will be diminished. On the other hand, long-lived low frequency components can tolerate poorer time resolution, but require effective frequency resolution. Low-frequency components, often determine the significant part of a signal's character and these properties will be best quantified if the frequency resolution is as satisfactory as possible. More references on the CWT can be found in Appendix B-A.

V. RESPIRATORY AND INHALER SOUNDS CLASSIFICATION

We provide the flow of the research in the topic we discussed, mainly with a chronological, pictorial representation of the machine learning methods, that we developed with the presented dataset and we evaluated the accuracy of each algorithm. We try to cover a large part of the existing material, so all points of interest need to be included to capture from one corner of the topic to the current status of the research and make the research of broad interest, but focusing only on an inhaler and respiratory sounds. The elements of the pipeline will be executed in parallel and in a time-sliced fashion, at some points. In some approaches, the data must be transformed to take advantage of the value it can deliver,

so it can continuously improve the accuracy of the models and achieve successful results [80]. We tried to have the appropriate data quality, reliability and accessibility. Metadata extraction is correlated with the captured data and provides descriptive and targeted information about the object and the data itself.

A. Classical machine learning algorithms for feature-based respiratory signals classification

1) *Decision Tree with CWT*: Chronologically, the first algorithm that was employed to identify actuation sounds was presented in [81] and utilized Decision Trees (DTs), with CWT for inhalation classification. The CWT was calculated using a Morlet Wavelet (MW) with an adjustable parameter of 20. A peak assessment routine was then employed to detect and assess peaks, exceeding a threshold $\theta_1 = 0.38$. Each peak was initially marked as a potential actuation plume. Power values were taken at specific time distance (56 ms), before and after the peak point, to observe if the power decreased by a given threshold ($\theta_2 = 25\%$) in comparison to the peak value, to flag it as an actuation plume. It was observed that the actuation acoustic signal was of a very small duration (100-150ms). The wavelet variance is calculated, so that different datasets may be compared at different scales:

$$V(a) = \frac{1}{n} \sum_{j=1}^n W^2(a, x_j) \quad (8)$$

where $W^2(a, x_j)$ is the squared wavelet coefficient, associated with scale a at data point x_j and n is the number of data points. From this definition, wavelet variance is a function of scale. Bradshaw and Spies [82] pointed out that "high values of wavelet variance, at a given scale, reflect the presence of a greater number of peaks or a greater intensity of the signal, or both".

2) *Quadratic Discriminant analysis*: In 2018, a Quadratic Discriminant Analysis (QDA) model was employed [83], for audio-based analysis of respiratory sounds. The algorithm was composed of two phases, training and testing, to automatically recognize the sound events. In both training and testing phases, the inhaler audio signal was band-pass filtered at 140 to 22000 Hz, to emphasize the events and to reduce the external noise. The audio signals were divided into frames of 40 ms duration with 20 ms overlap. The DC offset (mean amplitude displacement from zero) was removed from each frame. Thirty audio-based features from time and spectral domains were extracted, for each frame. The extracted features are: 12 MFCC's, 10 Linear Predictive Coding (LPC) coefficients, PSD, ZCR and a high frequency (over 15 kHz) power value, estimated using the CWT. Since the Flo-Tone device generates a harmonic sound during inhalation, a harmonic feature was also extracted. This harmonic feature was calculated as the peak value of the frame's auto-correlation function, searched in the range of 500–600Hz.

Classifying between two multivariate normal populations leads to the idea of discriminant analysis, which is essentially the Bayes classifier for the problem, that constructs a combination of the features. The features from two classes follow

multivariate normal distributions, with different means μ_i , with precision matrices $\Omega_i = \Sigma_i^{-1}$, with $i = 1, 2, \dots, Q(Y)$ (where $Q(Y)$ is the cardinal number of the set Y of the classes). In this, high dimensional setting, these matrices can be estimated only in presence of sparsity.

Consider observing training data (X_m, Y_m) , $m = 1, \dots, n$ where $X_m \in \mathfrak{X}$ and $Y_m \in \{0, 1, \dots, n\}$ and

$$X_m | \{Y_m = k\} \sim p_i(x), \text{ if } Y_m = i$$

for density p_i . A classification rule (or a classifier) ϕ is a map $\phi : \mathfrak{X} \rightarrow [0, \dots, Q(Y)]$, such that $\phi(x)$ stands for the probability of classifying a new observation to Class i . The misclassification rate of a classifier ϕ is given by $r(\phi) = \mathbb{E}[Y(1 - \phi(X)) + (1 - Y)\phi(X)]$.

The idea of the one-versus-the-rest method is as follows: to get a K -class classifier, first construct a set of binary classifiers C_1, C_2, \dots, C_K . Each binary classifier is first trained to separate one class from the rest and, then, the multi-class classification is carried out according to the maximal output, of the binary classifiers. Since the binary classifiers are obtained by training on different binary classification problems, it is unclear whether their real-valued outputs (before thresholding) are on comparable scales [84]. In practice, however, situations often arise where several binary classifiers assign the same instance to their respective class (or where none does). In addition, binary one-versus-the-rest classifiers has been criticized for dealing with somewhat asymmetric problems [84].

3) *Support Vector Machines*: Support Vector Machines (SVM) are based on statistical learning theory [85] and have shown to be one of the most robust supervised learning methods. Their simplicity comes from the fact that they apply a simple linear method to the data, but in a high-dimensional feature space are non-linearly related to the input space. In binary classification, only the decision boundaries of the first class are to be known and the rest (complement of first-class) is considered as second class, whereas in multi-class classification, several decision boundaries need to be calculated for this reason, which may lead to increase of error probability. SVM are highly accurate and able to model complex non-linear decision boundaries. The SVM classifier may be applied both to linearly and non-linearly separable data, with the use of kernel transformations. Specifically, it transforms the data to a higher dimension, from where it can identify a hyperplane that separates the data.

4) *Random Forest*: The Random Forest (RF) algorithm trains several tree-like classifiers [86] and aggregates results, by majority voting. The RF usually illustrates high accuracy and processing speed, though the correlation or/and independence of trees may affect the accuracy of the outcomes. The RF classifier draws n tree bootstrap samples from the original data and, among the variables, the best split is selected. The accuracy of RF overall depends on the strength of each tree and the correlation between any two trees. Each tree in RF can also be constructed by a bootstrap sample from the data, using a small set of randomly selected attributes.

5) *Adaboost*: Boosting was proposed by Freund and Schapire in 1990 [87]. It is an efficient instrument for improving the predictive ability of a learning system and a most

typical method in coordinating learning. Adaboost is the most common boosting algorithm. It usually employs decision tree models as weak learners and evaluates them sequentially [88]. Subsequent DTs are updated in favour of those samples misclassified by previous decision trees.

Preparing training sets $(x_1, y_1), \dots, (x_n, y_n) \cdot x_i \in X$, X represents a certain domain or instance space and each member is a training example, with a label. Initially, it was a two-class problem of learning. In going from two-class to multi-class classification, most boosting algorithms have been restricted to reducing the multi-class classification problem to multiple two-class problems, e.g. as shown in early works by Freund, Schapire, Singer, et al. [89]–[92] and Friedman, et al. [93], [94]. The weights of all the training examples are initially set to be $1/m$ equally. Adaboost conducts T times of iteration through repeatedly calling a weak learning algorithm. The weight of each instance would increase, while the training fails each time, so as to enable the weak learner to focus on the instance of failure, in training. As per D_t distribution, the weak learner finds appropriate weak hypothesis $h_t : X \rightarrow R$, thus, predicting function sequence is gained, at this point. In the simplest case, if the scope of each h_t is two-valued $\{-1, +1\}$, the task of the learner is to minimize the error. Combining T - weak hypotheses, the final predicting function (hypothesis) H is gained, after T times of circulation, with a weighted majority voting method. The learning accuracy rate of a single weak learner is not high enough [95], however, with the application of Boosting algorithm, the accuracy rate of the final result is to be improved. The Adaboost algorithm is described in detail in appendix A-B.

6) *Gaussian Mixture Models*: Gaussian Mixture Models (GMM's) can be employed to approximate any Probability Density Function (PDF), given a number of components. It is proposed a novel content based audio classification approach, for monitoring pMDI medication adherence [96], which exploits the separability of the Cepstrogram features, using a GMM classifier. GMMs are statistical models for representing normally distributed sub-populations, within an overall population and are used in many pattern recognition applications. For each class, a separate model is trained, by fitting the corresponding feature vectors to a GMM, with parameters $\{a_i, \mu_i, C_i\}$, $i \in \{1, \dots, K\}$, where K is the number of components, a_i is the mixture weight of component i , μ_i is the d -dimensional vector containing the mean values for each feature and C_i is the corresponding co-variance matrix. The Gaussian mixture density $p(\nu|\lambda_n)$ is modeled as a linear combination of multivariate Gaussian PDFs, where ν is a feature vector and λ_n is the GMM, corresponding to class n . In order to classify a test feature vector, we derive the $P(\nu|\lambda_n)$, for each class. The test feature vector is assigned to the class n , with the greatest likelihood $P(\nu|\lambda_n)$. An expectation maximization (EM) approach is utilized to derive the parameters $K_n, \{a_i, \mu_i, C_i\}$ for the GMM λ_n , corresponding to the class n that best fit the input data.

After the optimal parameters, for the GMMs, have been computed and given d the number of features, K the number of components of the i^{th} feature vector v_i and λ_n the GMM

of class n , we get:

$$P(v_i|\lambda_n) = \sum_{i=1}^K a_i^n p_i^n(v) \quad (9)$$

where a_i^n are the mixture weights to satisfy the constraint:

$$\sum_{i=1}^M a_i^n = 1, \quad a_i^n \leq 0 \quad (10)$$

Finally, and after the $P(v|\lambda_n)$ for the test feature vector v and for each class n is estimated, the test feature vector is assigned to the class n with the greatest likelihood. Then, we have the relevant feedback. This procedure lies in the assumption that the initial dataset was compiled by a small group of people. For the derivation of the GMM, through the EM approach, we refer to the appendix A-C.

B. Deep Learning Models

Neural Networks (NNs) have been employed in the past for a variety of classification problems and have shown significantly accurate results in medical applications [97], [98] and general audio classification problems [99], [100]. The CNNs can adapt to the characteristics of the training dataset and create a hierarchy of increasingly complex features [101], while at the same time, they illustrate relatively fast and consistent convergence in the training process. This model is robust in automatically learning the intrinsic patterns from the data, which can both prevent time-consuming manual feature engineering and capture hidden intrinsic patterns more effectively. Moreover, a CNN is more capable of discovering intricate patterns in high-dimensional data, compared with manual feature engineering. A pooling layer is introduced in each stage to merge similar features, reducing the feature dimension and dealing with some motif variations due to small signal variability (shifts and distortions).

1) *Convolutional Neural Network approaches:* In classical machine learning based direction, it is proposed an algorithmic methodology, using Convolutional Neural Networks (CNNs), intending to produce more accurate results, for real life environments, as opposed to controlled laboratory conditions with reduced levels of noise. This type of models has been established as a reliable, data-driven approach for time series and image classification [102], [103]. Also, the authors in [104] have demonstrated their accuracy and efficiency in classification tasks, while strengthening the basis for CNN architectures.

An important CNN approach [105], has a deep architecture that is consisted of two convolutional layers, of 16 1D kernels of size 100, followed by subsampling layers of size 2. Two fully connected layers of size 256 and 16, each of which was subjected to 50% dropout in the training process, lead to the output of two distinct states. For all layers of the CNN, RELU was selected as the activation function, in order to reduce the computational complexity of the algorithm. Furthermore, the initialization of the network's parameters was performed, using a random generator of uniform distribution. Finally the training of the 1D CNN utilized Adam and was based on

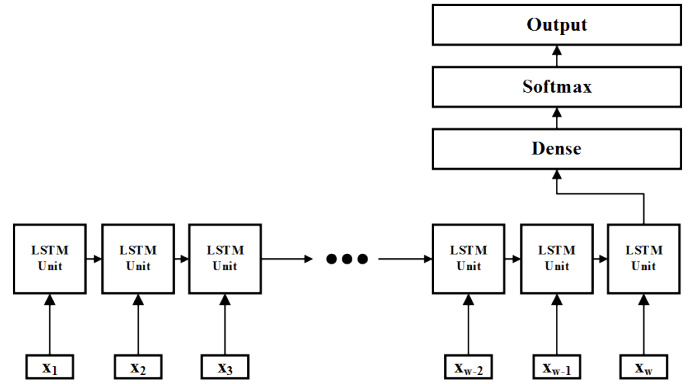


Fig. 3: Architecture of the LSTM network.

the categorical cross-entropy, between the predictions and the target values.

Later, a fast data-driven approach [106], [107] was proposed, based on 2D convolutional neural networks. The benefits according to the authors can be summarized in the following points: a) The presented approach is applied directly on the time domain to gain from reduced computational complexity. b) An extensive execution time evaluation study demonstrates that the presented approach is faster than most of the state-of-the-art methods. c) Convolutional deep sparse coding speeds up the computational graph, aiming to allow the real-time implementation. Specifically, the architecture utilizes three convolutional layers with each layer constituted by a max pooling layer and a dropout function [108]. The output is fed to a set of four dense layers. To compute the loss of each model, it is used categorical cross entropy. Furthermore, the stride is set to one and it was used zero padding to keep the shape of the output of each filter, constant. By processing an audio recording, a vector of n samples is created, reshaped in a two-dimensional array.

2) *LSTM analysis and implementation:* In this approach [109], deep layers were added to the network. The proposed sequential architecture, in Figure 3 consists, initially, of one layer of LSTM memory cells, with each one consisting of $h = 64$ units. After the LSTM input layer, a dropout layer [110] is introduced, in order to reduce overfitted parts after training, with dropout rate set to 0.3, followed by a flatten layer and a dense output layer, that returns a 4×1 vector. Finally, a softmax activation function is used. The model is optimized using binary cross-entropy loss [111] and the Adam optimizer [112].

The spectrogram was used as a tool to develop a classifier of inhaler sounds. It is swept across the temporal dimension, with a sliding window with length $w = 15$, moving at a step size equal to 1 window. In order to form the training instances, we segment \mathbf{S} into time windows of size $N_f \times T$ and assign a class to each one of them, according to the class of the central point of the window, as presented in Figure 1. Each training example \mathbf{W}_k is defined as:

$$\mathbf{W}_k \in \mathcal{R}^{N_f \times T} = (\mathbf{S}_{ij})_{\substack{1 \leq i \leq N_f \\ k-w \leq j \leq k}} \quad (11)$$

The training set is organized in minibatches \mathbf{B} , so that $\mathbf{B} \in \mathcal{R}^{b \times (T \times N_F)}$ (with $b = 25$ in our experiments). The input tensor can be defined as $\mathbf{X} \in \mathcal{R}^{n \times w \times F}$, where $n = 25$ is the minibatch size, $w = 25$ is the window size and $F = 42$ is the dimension of spectrogram feature vector.

Extensive hyper-parameter optimization took place, to define the number of hidden units, the number of dropout rate and the minibatch size. By observing the performance of the network on the validation set, we stopped training at 70 epochs, to avoid over-fitting. The testing loss increases and the average testing accuracy stabilizes after around 70 epochs.

VI. COMPARATIVE ANALYSIS OF THE ALGORITHMIC APPROACHES

A. Simulation setup and validation settings

The Respiratory and Drug Actuation Benchmark is a publicly available benchmark suite² employed to carry the following study. We compare the classification performance of the aforementioned important and widely used machine learning and deep learning algorithms, namely the Random Forests (RF), Support Vector Machines (SVM), Adaboost, Convolutional Neural Networks (CNNs) and Recurrent Neural Networks (LSTMs). They were evaluated with spectrogram, cepstrogram and MFCC features. CNNs were directly applied on timeseries values aiming to demonstrate their capability to provide dependable solutions at lower execution times.

A main differentiation parameter in validation comes from the availability of previous recordings, from a specific individual. It is expected that prior information can increase the classification accuracy, however it puts additional burden in the usage of the monitoring system, since it requires the collection of data every time a new patient wants to test the framework.

Firstly, we consider the *Multi Subject* modeling approach, denoted as *MultiSubj*. In this case, the recordings of all subjects are used to form a large dataset, which is divided in five equal parts used to perform five-fold cross-validation, thereby allowing different samples from the same subject to be used in training and test set, respectively. This validation scheme was followed in previous work [106] and thus performed, also, here for comparison purposes.

The second case includes the *Single Subject* setting, in which the performance of the classifier is validated through training and testing, within each subject's recordings. We denote such models, as *SingleSubj*. Specifically, the recordings of each subject are split in five equal parts, to perform cross-validation. The accuracy is assessed for each subject separately and, then, the overall performance of the classifier is calculated by averaging the three individual results.

The third evaluation setting refers to the case, when no previous recordings for the testing subject are available, thus samples from other subjects are used. This is the *leave-one-subject-out (LOSO)* approach that illustrates how well the trained network can generalize to individuals that it never saw before, during training. *LOSO* models facilitate the use

of the monitoring system since they don't require a data pre-collection phase and they also have the lowest risk of over-fitting. However, if the inter-subject variability is high, they might not adapt well, especially if the number of training subjects is small, as in our case. With this approach we use the recordings of two subjects for training and the recordings of the third subject for testing. This procedure is completed, when all subjects have been used for testing, and the accuracy is averaged to obtain the overall performance of the classifiers.

Furthermore, a new parameter was brought into the comparison, the testing dataset mixing. A non mixed setup means that each audio segment, in the testing set, consists of a single class, but in a mixed setup each testing set sample emanates from a sliding window that naturally includes parts belonging to multiple classes. In this case, the class of an audio segment is the class of the central sample.

B. Key performance indicators

Table I summarizes the classification accuracy for drug, exhalations and inhalations across all validation setups. Out of a superficial examination no method is outright better, but key performance indicators need to be established. Multi-subject and single-subject settings indicate how successful the classifier is, if the user has participated previously in the sampling process. *LOSO* setting is the closest to real situation setting, since a commercial classifier would not assume that a new user had already submitted samples to the training process. Even though a feedback loop can improve accuracy [96] such a process cannot be a prerequisite. As a result, *LOSO* performance is the most representative. Furthermore, between mixed and non-mixed, the first is closer to real situation, since the non-mixed setup assumes that the position of audio segments containing a certain audio event is known before the classifier is applied. Furthermore, tables III and IV present the performance of classifiers in drug detection and exhalation-inhalation differentiation. Again, the *LOSO*-mixed setup is the most representative of reality. In short the key performance indicators can be summarized in the following list:

- Non-mixed multisubject accuracy to exceed 96% (Table I)
- The highest non-mixed *LOSO* accuracies should be highlighted (Table I)
- The highest mixed multisubject accuracies should be highlighted (Table I)
- The highest mixed *LOSO* accuracies should be highlighted (Table I)
- The highest drug analysis mixed and non-mixed sensitivity should be highlighted (Table III)

Metrics to measure the performance of the compared classifiers are accuracy, sensitivity and specificity. For the sake of self completeness $\text{accuracy} = \frac{TP+FP}{TP+FP+TN+FN}$, $\text{sensitivity} = \frac{TP}{TP+FN}$, $\text{specificity} = \frac{TN}{TN+FP}$, where:

TP = The number of positive correct identifications

TN = The number of negative correct identifications

FP = The number of positive incorrect identifications

FN = The number of negative incorrect identifications

²<https://gitlab.com/vvr/monitoring-medication-adherence/rda-benchmark>

C. Results

Close inspection of Table I reveals that no method clearly outperforms the others. The performance of data driven approaches largely depends on the dataset and the pre-processing steps, however, since all the approaches were trained with the same dataset we are able to quantify which of them can capture in a more efficient way, the individual characteristics. In general, for all methodologies the multisubject approach yields the highest score. This means that if a user's data have been included in the training process, the success probability climbs to a level near to 100%. Given the KPIs, defined in the previous section, LSTM-SPECT, GMM-CEPST, SVM-SPECT and SVM-MFCC achieve the highest accuracies, greater than 96%, in the multisubject setting.

Examining the LOSO accuracy, which represents better real life scenarios, we can distinguish in the non-mixed setup the LSTM-SPECT and CNN-TIME approaches. It is also notable that RF-MFCC captures 100% drug detection accuracy. The rest of the approaches demonstrate high variation of performance, across classes. Another notable point is the LOSO mixed setup, where we assume a random window selection process, allowing multiple classes to be present within the same window. It is remarkable that RF-SPECT, RF-MFCC, ADABOOST-MFCC and LSTM-SPECT demonstrate more than 70% detection accuracy for all classes. However, the results of this table reveal that no method can easily tackle the real life scenario challenge.

Further insight is provided by Table III. Measuring sensitivity is highly important since it reveals the rate of true positive in drug detection. In the multi-subject, non-mixed setup, GMM-MFCC (100.0%), LSTM-SPECT (98.8%), SVM-MFCC (94.975%) SVM-SPECT(94.059%), GMM-SPECT (93.401%) and RF-SPECT (94.03%) are viable solutions. However, in the LOSO non-mixed setup the outcome is different with RF-CEPST (77.778%), GMM-SPECT (83.33%), CNN (77.7%) and LSTM-SPECT (77.941%) outperforming other methods. Reaching common grounds RF-CEPST, LSTM-SPECT are quite balanced solutions, since they, also, cover the aforementioned criteria. Furthermore, on LOSO mixed sensitivity is low for every method. The GMM-SPECT approach is the highest one only to yield 21.15%. Regarding inhalation-exhalation differentiation, the results are presented in Table IV, all methods perform adequately, with a few of them achieving a near to 98% performance, in LOSO mixed setup. Comparison with literature is not easily possible since different dataset and pre-processing steps highly affect the accuracy. Table II presents the self-reported accuracy of other studies.

To summarize, a combination of methods can sufficiently answer the question of which method better differentiates inhaler sounds and the performance highly depends on the dataset annotation and on the dataset size. In all cases, it helps the scenarios when the patient is also a participant. The latter was also proven in a previous study, that proposed a relevance feedback mechanism [96].

VII. DISCUSSION AND FUTURE CONSIDERATIONS

The pressurized metered dose inhaler (pMDI) is the most commonly used inhaler, with total worldwide sales of pMDI products reaching over \$2 billion per year [113]. Studies have reported that over 50% of patients are prone to not adhering to the correct inhaler technique [114]. It has been stated that acoustics can be employed to detect and recognize dry powder inhaler sounds [115]. Almost 4 decades ago, the earliest investigations into poor inhaler sufficiency in patients using pMDIs, indicated that poor technique was likely to be associated with less than the highest quality of response to the therapy [116], [117]. Several studies have since intimated a strong connection between poor inhaler adequacy and patient outcomes, on a larger scale [118], including higher rates of hospital access and emergency room attendance [119]. By providing suitable feedback to medical staff and guiding patients to improve their inhaler usage technique, could facilitate efficient self-management of obstructive respiratory diseases, allowing patients to avoid dangerous exacerbation events [108]. Asthma is almost in the center of the wave of digital health developments, as it requires systematic attention of both health care specialist doctors and patients [120]. Employing acoustic signal processing methods, the aforementioned algorithms were developed to accurately identify drug actuations, from pMDI's. As science and technology evolve and modern sensing components are becoming more available, a continual improvement process of inhalers, with an extended range of monitoring capabilities, holds the promise to further optimize asthma self-management. These methods provide an opportunity to enhance clinical education, by providing informative feedback to patients, which may contribute to improving respiratory health. Future work will consist of identifying pMDI inhalations to monitor actuation coordination technique and provide patient feedback, regarding drug delivery using acoustic methods. The accurate estimation of the parameters would be of significant clinical benefit to both patients and healthcare professionals, by enhancing precision medicine for chronic respiratory diseases. Ultimately, this work aims to prevent common mistakes, leading to potential upcoming dangerous events, such as exacerbation and hospitalization.

VIII. CONCLUSIONS

Asthma forms an important socioeconomic burden, both in terms of medication costs and disability adjusted life years. The accurate and timely assessment of the state of asthma is the fundamental basis of digital health approaches and, also, is the most significant factor towards the preventive and efficient management of the disease. The necessity of inhaled medication offers a basic platform, upon which, modern technologies can be integrated, namely the inhaler device system itself. The control of asthma is a complex and multiparametric issue, that is greatly affected not only by physiological and environmental parameters, but, also, the psychological state of patients and their cultural and socioeconomic background. Indicative of the complexity of the asthma disease is the diversity of its prevalence around the world. All the above outline the need to increase the active involvement of patients in modern treatment

TABLE I: Accuracy summarization

		Multi subject *			Single subject			LOSO **		
		Drug	Exhale	Inhale	Drug	Exhale	Inhale	Drug	Exhale	Inhale
Random Forests										
Spect	Non-mixed	97.927	92.097	94.984	98.907	92.689	93	70	80.591	91.597
	Mixed	84.399	87.343	89.928	83.899	89.498	88.246	89.024	73.445	83.788
Cepst	Non-mixed	91.192	96.266	96.238	93.989	94.987	95	70	86.92	94.958
	Mixed	62.588	92.414	84.287	64.35	90.53	84.648	53.049	77.674	78.549
MFCC	Non-mixed	95.337	95.645	96.552	96.175	94.778	96	100	83.122	91.597
	Mixed	79.221	92.831	82.108	78.845	91.861	80.921	75.61	77.071	75.693
GMM										
Spect	Non-mixed	95.337	84.516	95.611	96.175	83.29	95	40	77.637	94.118
	Mixed	85.803	74.293	93.079	86.017	78.715	92.384	72.866	63.384	86.997
Cepst	Non-mixed	95.337	95.617	95.925	95.628	95.251	96	50	80.169	60.504
	Mixed	72.984	90.183	75.486	72.172	87.908	76.566	42.683	64.026	32.007
MFCC	Non-mixed	5.699	99.355	60.815	10.929	98.172	85	0	96.203	31.933
	Mixed	11.018	97.04	39.334	0.235	97.146	47.214	0	94.451	26.545
ADABoost										
Spect	Non-mixed	96.373	94.194	96.238	96.721	94.517	92.5	70	78.903	86.555
	Mixed	84.399	89.81	90.665	80.756	87.467	86.23	89.024	71.282	76.937
Cepst	Non-mixed	93.264	96.916	96.865	93.443	93.668	94	70	89.873	94.958
	Mixed	66.481	92.149	83.862	67.077	89.463	81.516	41.768	77.745	77.635
MFCC	Non-mixed	97.927	96.774	97.179	93.989	93.473	94.5	90	85.232	74.79
	Mixed	80.93	93.766	84.177	75.813	88.733	79.546	69.207	78.285	68.986
SVM										
Spect	Non-mixed	98.446	98.548	95.298	98.907	97.389	94.5	90	97.468	94.958
	Mixed	85.711	98.381	88.947	85.588	97.342	87.056	90.854	97.245	84.68
Cepst	Non-mixed	94.301	96.916	96.552	96.175	96.042	97	90	67.932	72.269
	Mixed	73.196	91.68	83.494	75.204	91.6	84.671	58.232	57.366	52.148
MFCC	Non-mixed	97.927	96.613	96.552	97.814	95.822	96	100	65.823	78.992
	Mixed	84.876	91.739	83.772	85.062	91.816	83.375	78.659	57.748	69.67
LSTM										
Spect	Non-mixed	99.085	96.483	97.353	98.808	94.975	98.889	100	88.027	88.422
	Mixed	82.047	89.562	91.959	82.056	90.085	89.832	90.909	79.261	82.53
CNN										
Time	Non-mixed	83.753	96.537	97.19	88.061	92.264	96.322	63.636	91.826	98.066
	Mixed	65.316	88.828	85.85	65.056	83.73	87.789	66.768	86.707	93.481
*Multi-subject non-mixed setup accuracies are highlighted if value >96%.										
**LOSO mixed setup accuracies are highlighted if value >70%										

TABLE II: Relevant state of the art.

	Drug	Inhale	Exhale
Holmes et al. (2012)	89	-	-
Holmes et al. (2013-14)	92.1	91.7	93.7
Taylor et al. (2017) / QDA	88.2	-	-
Taylor et al. (2017) / ANN	65.6	-	-

methodologies and to use modern technologies, so as to create easy-to-use tools for safe and effective self-management. A fundamental step in this direction is the creation of a sensing framework, that could provide accurate information, about the health of patients and help their doctors understand any possible difficulty, that prevents patients from using their inhaled medication correctly. This need for the modernization of inhaler devices has stimulated the research and commercial interest for their enhancement with novel sensing capabilities and has led to a number of approaches, that focus mainly on the detection of inhaler actuations. The modern adherence monitoring environment has also been analyzed in other studies, addressing important related issues, such as the interpretation of results and the design of interventions that promote adherence.

APPENDIX A MACHINE LEARNING ALGORITHMS

A. Support vector machines

For a decision hyper-plane $\mathbf{x}^T \mathbf{w} + b = 0$ to separate the two classes $P = \{(\mathbf{x}_i, 1)\}$ and $N = \{(\mathbf{x}_i, -1)\}$, it has to satisfy

$$y_i(\mathbf{x}_i^T \mathbf{w} + b) \geq 0$$

for both $\mathbf{x}_i \in P$ and $\mathbf{x}_i \in N$. Among all such planes satisfying this condition, we want to find the optimal one H_0 that separates the two classes with the maximal margin (the distance between the decision plane and the closest sample points). The optimal plane should be in the middle of the two classes, so that the distance from the plane to the closest point on either side is the same. We define two additional planes H_+ and H_- that are parallel to H_0 and go through the point closest to the plane on either side:

$$\mathbf{x}^T \mathbf{w} + b = 1, \quad \text{and} \quad \mathbf{x}^T \mathbf{w} + b = -1$$

All points $\mathbf{x}_i \in P$ on the positive side should satisfy

$$\mathbf{x}_i^T \mathbf{w} + b \geq 1, \quad y_i = 1$$

and all points $\mathbf{x}_i \in N$ on the negative side should satisfy

$$\mathbf{x}_i^T \mathbf{w} + b \leq -1, \quad y_i = -1$$

These can be combined into one inequality:

$$y_i(\mathbf{x}_i^T \mathbf{w} + b) \geq 1, \quad (i = 1, \dots, m)$$

The equality holds for those points on the planes H_+ or H_- . Such points are called *support vectors*, for which

$$\mathbf{x}_i^T \mathbf{w} + b = y_i$$

i.e., the following holds for all support vectors:

$$b = y_i - \mathbf{x}_i^T \mathbf{w} = y_i - \sum_{j=1}^m \alpha_j y_j (\mathbf{x}_i^T \mathbf{x}_j)$$

Moreover, the distances from the origin to the three parallel planes H_- , H_0 and H_+ are, respectively, $|b - 1|/\|\mathbf{w}\|$, $|b|/\|\mathbf{w}\|$, and $|b + 1|/\|\mathbf{w}\|$, and the distance between planes H_- and H_+ is $2/\|\mathbf{w}\|$. Our goal is to maximize this distance, or equivalently, to minimize the norm $\|\mathbf{w}\|$. Now the problem of finding the optimal decision plane in terms of \mathbf{w} and b can be formulated as:

$$\text{minimize} \quad \frac{1}{2} \mathbf{w}^T \mathbf{w} = \frac{1}{2} \|\mathbf{w}\|^2 \quad (\text{objective function})$$

$$\text{subject to} \quad y_i(\mathbf{x}_i^T \mathbf{w} + b) \geq 1, \quad \text{or} \quad 1 - y_i(\mathbf{x}_i^T \mathbf{w} + b) \leq 0,$$

($i = 1, \dots, m$). Since the objective function is quadratic, this constrained optimization problem is called a quadratic program (QP) problem. (If the objective function is linear instead, the problem is a linear program (LP) problem). This QP problem can be solved by Lagrange multipliers method to minimize the following

$$L_p(\mathbf{w}, b, \alpha) = \frac{1}{2} \|\mathbf{w}\|^2 + \sum_{i=1}^m \alpha_i (1 - y_i(\mathbf{x}_i^T \mathbf{w} + b))$$

with respect to \mathbf{w} , b and the Lagrange coefficients $\alpha_i \geq 0$ ($i = 1, \dots, \alpha_m$). We let

$$\frac{\partial}{\partial \mathbf{w}} L_p(\mathbf{w}, b) = 0, \quad \frac{\partial}{\partial b} L_p(\mathbf{w}, b) = 0$$

These lead, respectively, to

$$\mathbf{w} = \sum_{j=1}^m \alpha_j y_j \mathbf{x}_j, \quad \text{and} \quad \sum_{i=1}^m \alpha_i y_i = 0$$

Substituting these two equations back into the expression of $L(\mathbf{w}, b)$, we get the *dual problem* (with respect to α_i) of the above *primal problem*:

$$\text{maximize} \quad L_d(\alpha) = \sum_{i=1}^m \alpha_i - \frac{1}{2} \sum_{i=1}^m \sum_{j=1}^m \alpha_i \alpha_j y_i y_j \mathbf{x}_i^T \mathbf{x}_j$$

$$\text{subject to} \quad \alpha_i \geq 0, \quad \sum_{i=1}^m \alpha_i y_i = 0$$

The dual problem is related to the primal problem by:

$$L_d(\alpha) = \inf_{(\mathbf{w}, b)} L_p(\mathbf{w}, b, \alpha)$$

i.e., L_d is the greatest lower bound (infimum) of L_p for all \mathbf{w} and b . Solving this dual problem (an easier problem than the primal one), we get α_i , from which \mathbf{w} of the optimal plane can be found. Those points \mathbf{x}_i on either of the two planes H_+ and H_- (for which the equality $y_i(\mathbf{w}^T \mathbf{x}_i + b) = 1$ holds) are called *support vectors* and they correspond to positive Lagrange multipliers $\alpha_i > 0$. The training depends only on the support vectors, while all other samples away from the planes H_+ and H_- are not important. For a support vector \mathbf{x}_i (on the H_- or H_+ plane), the constraining condition is

$$y_i (\mathbf{x}_i^T \mathbf{w} + b) = 1 \quad (i \in sv)$$

TABLE III: Comparative performance of methods for drug inhalation recognition

		Multi subject *			Single subject			LOSO **		
		Accuracy	Specificity	Sensitivity	Accuracy	Specificity	Sensitivity	Accuracy	Specificity	Sensitivity
Random Forests										
Spect	Non-mixed	99.023	99.721	94.03	98.473	99.782	92.347	98.473	99.414	58.333
	Mixed	98.677	99.638	66.172	98.266	99.458	69.083	99.051	99.967	22.155
Cepst	Non-mixed	98.034	98.817	92.147	97.736	98.802	92.473	99.046	99.417	77.778
	Mixed	98.39	99.139	64.74	97.798	98.81	66.476	99.117	99.861	17.262
MFCC	Non-mixed	98.717	99.375	93.878	98.293	99.243	93.617	98.473	100	55.556
	Mixed	97.844	99.515	51.383	97.38	99.284	56.831	97.831	99.927	9.553
GMM										
Spect	Non-mixed	98.656	99.375	93.401	98.383	99.244	94.118	98.282	98.839	57.143
	Mixed	98.613	99.67	64.423	98.074	99.528	65.352	99.124	99.92	21.15
Cepst	Non-mixed	98.342	99.369	91.089	98.279	99.129	94.086	98.855	99.035	83.333
	Mixed	98.148	99.374	56.92	97.749	99.066	63.326	99.281	99.831	18.494
MFCC	Non-mixed	88.882	88.807	100	84.097	84.893	58.824	97.519	98.081	0
	Mixed	97.6	97.983	38.465	96.775	96.775	100	99.159	99.705	0
ADABoost										
Spect	Non-mixed	98.9	99.514	94.416	98.293	99.35	93.158	97.901	99.411	46.667
	Mixed	98.723	99.639	67.24	98.213	99.353	69.144	98.506	99.967	15.145
Cepst	Non-mixed	98.342	99.093	92.784	97.645	98.694	92.432	98.473	99.414	58.333
	Mixed	98.377	99.227	63.28	97.483	98.896	59.881	98.852	99.827	11.129
MFCC	Non-mixed	99.145	99.722	94.975	98.293	98.821	95.556	94.847	99.796	25.714
	Mixed	97.959	99.555	53.065	97.419	99.183	57.666	96.987	99.907	6.489
SVM										
Spect	Non-mixed	99.084	99.791	94.059	98.922	99.783	94.764	99.237	99.805	75
	Mixed	98.43	99.668	60.73	98.008	99.513	64.443	98.452	99.973	14.893
Cepst	Non-mixed	98.526	99.232	93.333	98.46	99.237	94.624	95.42	99.797	28.125
	Mixed	98.061	99.378	55.242	97.442	99.163	58.053	97.419	99.874	6.49
MFCC	Non-mixed	99.145	99.722	94.975	98.922	99.568	95.722	97.137	100	40
	Mixed	97.574	99.645	47.821	97.36	99.492	56.038	97.379	99.936	8.264
LSTM										
Spect	Non-mixed	99.803	99.903	98.858	99.711	99.814	99.044	99.656	100	77.941
	Mixed	98.626	99.629	61.938	98.377	99.462	68.281	98.942	99.977	17.778
CNN										
Time	Non-mixed	99.666	99.842	81.86	99.574	99.822	83.727	99.978	99.985	77.778
	Mixed	97.879	99.196	52.323	97.573	98.831	61.853	98.6	99.901	13.059
*Multi-subject non-mixed setup accuracies are highlighted if value >60%.										
**LOSO mixed setup accuracies are highlighted if value >15%										

TABLE IV: Exhalation Inhalation differentiation analysis.

		Multi subject			Single subject			LOSO		
		Accuracy	Specificity	Sensitivity	Accuracy	Specificity	Sensitivity	Accuracy	Specificity	Sensitivity
Random Forests										
Spect	Non-mixed	98.646	98.377	98.789	98.543	98.413	98.611	99.01	99.091	98.964
	Mixed	98.25	98.325	98.207	97.953	97.877	97.994	98.619	100	97.775
Cepst	Non-mixed	98.793	98.714	98.833	98.39	98.446	98.361	98.762	99.123	98.565
	Mixed	97.511	98.827	96.869	97.586	98.323	97.214	97.613	99.699	96.494
MFCC	Non-mixed	98.794	98.718	98.833	98.579	98.462	98.641	99.029	99.091	98.995
	Mixed	97.656	98.729	97.146	97.515	98.214	97.183	98.436	100	97.614
GMM										
Spect	Non-mixed	98.339	96.825	99.242	94.963	89.623	98.457	98.997	97.391	100
	Mixed	97.342	95.658	98.529	96.223	93.019	98.393	98.59	98.365	98.76
Cepst	Non-mixed	98.786	98.71	98.826	98.574	98.462	98.634	98.868	98.63	98.958
	Mixed	97.384	98.764	96.765	96.379	98.545	95.383	98.053	100	97.533
MFCC	Non-mixed	89.011	98.98	86.275	94.627	98.837	92.84	76.879	97.436	74.267
	Mixed	84.178	98.758	81.513	81.274	97.849	77.781	75.19	100	72.425
Adaboost										
Spect	Non-mixed	98.671	98.397	98.816	98.029	97.884	98.103	98.976	99.038	98.942
	Mixed	98.266	98.329	98.231	97.336	97.527	97.233	98.343	100	97.389
Cepst	Non-mixed	98.8	98.722	98.841	97.838	97.409	98.066	99.088	99.123	99.07
	Mixed	97.506	98.716	96.915	97.03	97.474	96.811	98.047	100	97.01
MFCC	Non-mixed	98.806	98.726	98.847	98.205	98.438	98.082	98.98	98.889	99.02
	Mixed	97.826	98.672	97.417	96.094	96.475	95.909	98.373	100	97.607
SVM										
Spect	Non-mixed	98.706	98.382	98.867	98.424	97.927	98.677	98.851	98.261	99.142
	Mixed	97.738	97.881	97.667	97.41	96.789	97.716	97.92	98.824	97.495
Cepst	Non-mixed	98.799	98.718	98.841	98.587	98.477	98.645	98.406	98.851	98.171
	Mixed	98.054	99.043	97.569	97.801	98.519	97.443	96.333	100	94.605
MFCC	Non-mixed	98.909	98.718	99.008	98.589	98.462	98.656	98.814	98.947	98.734
	Mixed	98.094	98.797	97.747	97.992	98.523	97.731	97.348	100	95.671
LSTM										
Spect	Non-mixed	98.783	98.868	98.738	99.11	98.451	99.477	97.061	98.955	96.124
	Mixed	98.182	98.364	98.082	97.794	98.291	97.53	96.057	99.769	94.07
CNN										
Time	Non-mixed	98.121	97.39	98.528	97.69	97.06	98.046	99.055	99.228	98.951
	Mixed	97.553	98.133	97.249	96.897	96.776	96.966	99.296	100	98.885

here sv is a set of all indices of support vectors \mathbf{x}_i (corresponding to $\alpha_i > 0$). Substituting

$$\mathbf{w} = \sum_{j=1}^m \alpha_j y_j \mathbf{x}_j = \sum_{j \in sv} \alpha_j y_j \mathbf{x}_j$$

we get

$$y_i \left(\sum_{j \in sv} \alpha_j y_j \mathbf{x}_i^T \mathbf{x}_j + b \right) = 1$$

Note that the summation only contains terms corresponding to those support vectors \mathbf{x}_j with $\alpha_j > 0$, i.e.

$$y_i \sum_{j \in sv} \alpha_j y_j \mathbf{x}_i^T \mathbf{x}_j = 1 - y_i b$$

For the optimal weight vector \mathbf{w} and optimal b , we have:

$$\begin{aligned} \|\mathbf{w}\|^2 &= \mathbf{w}^T \mathbf{w} = \sum_{i \in sv} \alpha_i y_i \mathbf{x}_i^T \sum_{j \in sv} \alpha_j y_j \mathbf{x}_j \\ &= \sum_{i \in sv} \alpha_i (1 - y_i b) = \sum_{i \in sv} \alpha_i - b \sum_{i \in sv} \alpha_i y_i \\ &= \sum_{i \in sv} \alpha_i \end{aligned}$$

The last equality is due to $\sum_{i=1}^m \alpha_i y_i = 0$ shown above. Recall that the distance between the two margin planes H_+ and H_- is $2/\|\mathbf{w}\|$, and the margin, the distance between H_+ (or H_-) and the optimal decision plane H_0 , is

$$\frac{1}{\|\mathbf{w}\|} = \left(\sum_{i \in sv} \alpha_i \right)^{-1/2}$$

B. Adaboost

Let's assume N samples $x_i \in X$, $i = \{1, \dots, N\}$ with corresponding labels $y_i \in Y = \{-1, +1\}$ are given and used as a training set $(x_1, y_1), (x_2, y_2), \dots, (x_n, y_n)$.

Initially set up a weight $D(i)$ and make $D(i) = 1/N$ and then iterate for $t = 1, 2, \dots, T$, where T is a parameter representing the maximum circulation times of training. For T -training, firstly, the weight distributing on the sample $\{X_i, Y_i\}$ is recorded as $D_t(i)$ while the T -th iteration happens and as per the distribution D_t the weak learner finds its weak hypothesis $h_t : X \rightarrow \{+1, -1\}$ and adjusts distribution. Secondly, the error rate in computing h_t : $\varepsilon_t = \sum_{i=1}^N D_t(x_i) [h_t(x_i) \neq y_i]$. Thirdly, compute the weight of weak classifier based on the error rate: $\alpha_t = (1/2) \ln((1 - \varepsilon_t)/\varepsilon_t)$. Fourthly, update the sample weight: $D_{t+1}(x_i) = \frac{D_t(x_i)}{Z_t} \exp(-\alpha_t y_i h_t(x_i))$ among which, $Z_t = \sum_{i=1}^N D_t(x_i) \exp(-\alpha_t y_i h_t(x_i))$ Z_t is a standardized factor that meets the probability distribution. T -weak classifiers are gained after T times of circulation, and a strong classifier $H(x) = \text{sign}\left(\sum_{t=1}^T \alpha_t h_t(x)\right)$ is gained after adding to the updated weight [55].

C. GMM

In the GMM classifier, the Gaussian mixture density of each d -dimensional feature vector v is modeled as a linear combination of multivariate Gaussian PDFs with the general form:

$$p(v|\theta_i) = \frac{1}{(2\pi)^{\frac{d}{2}} |C_i|^{\frac{1}{2}}} e^{-\frac{1}{2}(v-\mu_i)^T C_i^{-1}(v-\mu_i)} \quad (12)$$

where $\theta_i = (\mu_i, C_i)$ are the parameters of component i , including the mean feature vector μ_i and the $d \times d$ covariance matrix C_i , and $|C_i|$ is the determinant of C_i . The complete set of parameters for a mixture model with K components is $\Theta = \{\alpha_1, \dots, \alpha_K, \theta_1, \dots, \theta_K\}$ Each GMM model λ_n for class n is parameterized as follows:

$$\lambda_n = \{a_k^n, \mu_k^n, C_k^n\} \quad (13)$$

where $k = 1, \dots, K$. It is important to note that each multivariate Gaussian pdf is completely defined if we know θ .

At this point we analyze the expectation-maximization (EM) algorithm employed to compute the GMM parameters. The membership weight of data point v in component k given parameter Θ is defined as:

$$w_{ik} = \frac{p_k(v_i, \theta_k) a_k}{\sum_{m=1}^K p_m(v_i | \theta_m) a_m} \quad (14)$$

for all components k , $1 \leq k \leq K$ and all data samples i , $1 \leq i \leq N$. In each iteration of the EM algorithm for Gaussian Mixtures we deploy an E-step and an M-step. At E-Step we compute w_{ik} for all feature vectors v_i and all mixture components k . At M-Step we calculate the new parameters. Given $N_k = \sum_{i=1}^N w_{ik}$ the sum of membership weights for the k -th component we get the mixture weights:

$$a_k^{new} = \frac{N_k}{N}, \quad 1 \leq k \leq K \quad (15)$$

The updated mean:

$$\mu_k^{new} = \frac{1}{N_k} \sum_{i=1}^N w_{ik} v_i, \quad 1 \leq k \leq K \quad (16)$$

and the updated covariance:

$$C_k^{new} = \frac{1}{N_k} \sum_{i=1}^N w_{ik} (v - \mu_i)^T (v - \mu_i) \quad (17)$$

The termination criteria for the EM is the following:

$$\log l(\Theta)_{t+1} - \log l(\Theta)_t \leq \epsilon \quad (18)$$

where the log-likelihood, defined as $\log l(\Theta) = \sum_{i=1}^N \log p(v_i | \Theta)$ and ϵ is a small user-defined scalar value. In order to find the best fit for the data, we compute the GMM for 1 to $d = 40$ components iterating over full and diagonal covariance matrices, where d is the size of each feature vector v . With the generation of each model we estimate the Bayesian Information Criteria (BIC). The model with the lowest BIC best fits the input data.

APPENDIX B FEATURE EXTRACTION

A. CWT

In theory, it is assumed that continuous signal $x(t)$ can be approximated perfectly by a_n and ψ_n , but in reality this is often not true. Let us consider a real signal $x(t)$ and its approximation $\hat{x}(t)$, which can be perfectly approximated by a_n and ψ_n . The approximation error is defined as the difference between $x(t)$ and $\hat{x}(t)$. This results in an error function, which is used as a measure for the overall error. Therefore the sum of the remaining squared inner products is calculated (2-norm) and is used as a measure for the error (ϵ).

$$\epsilon[M] = \|x(t) - \hat{x}(t)\|^2 = \sum_{n=M}^{+\infty} \left| \langle x(t), \psi_n(t) \rangle \right|^2 \quad (19)$$

with

$$\hat{x}(t) = \sum_{n=0}^{M-1} \langle x(t), \psi_n(t) \rangle \psi_n \quad (20)$$

If the number of terms M is increased the error becomes smaller i.e. when M goes to $+\infty$ then the approximation error goes to zero. The rate that determines how fast $\epsilon[M]$ goes to zero with increasing M is called the decay rate and says something about how well a certain frame can approximate a signal. To be “admissible” as a wavelet, this function must have zero mean and be localized in both time and frequency space (Farge 1992) [121].

The Continuous Wavelet Transformation (CWT) was introduced almost 3 decades ago, in order to overcome the limited time-frequency localization of the FFT [122] for non-stationary signals and was found to be suitable in multiple applications [122], [123]. It is similar to the human ear which exhibits similar time-frequency resolution characteristics [124], [125]. While the Fourier Transform decomposes a signal into infinite length sines and cosines, effectively losing all time-localization information, the CWT’s basis functions are scaled and shifted versions of the time-localized mother wavelet. The CWT of $x(t)$ at any scale s and position u is the projection of x on the corresponding wavelet atom ψ , as described in the following formula:

$$W_{\psi}^x(u, s) = \langle x, \psi_{u,s} \rangle = \int_{-\infty}^{+\infty} x(t) \frac{1}{\sqrt{s}} \psi^* \left(\frac{t-u}{s} \right) dt \quad (21)$$

It represents one-dimensional signals by highly redundant time-scale images in (u, s) . The CWT is an excellent tool for mapping the changing properties of non-stationary signals. The CWT consists of N spectral values for each scale used, each of these requiring an IFFT. The computational load of the CWT and its memory requirements are thus considerable. The benefit from this high measure of redundancy in the CWT is an accurate time-frequency spectrum. Unlike a Fourier decomposition which always uses complex exponential (sine and cosine) basis functions, a wavelet decomposition uses a time-localized oscillatory function as the analyzing or mother wavelet. The mother wavelet is a function that is continuous in both time and frequency and serves as the source function from which scaled and translated basis functions are constructed. The mother wavelet can be complex or real and it, generally, includes an adjustable parameter which controls the properties of the localized oscillation.

APPENDIX C TABLES

Tables V to XVI present in detail the classification outcomes for all methods, evaluation setups and classes. The aforementioned tables were used to derive tables in the results section

REFERENCES

- [1] World health organization asthma. fact sheet no 307. [Online]. Available: <http://www.who.int/mediacentre/factsheets/fs307/en/>
- [2] European lung white book. adult asthma. [Online]. Available: <http://www.erswhitebook.org/chapters/adult-asthma/>
- [3] European lung white book. childhood asthma. [Online]. Available: <http://www.erswhitebook.org/chapters/childhood-asthma/>
- [4] M. R. DiMatteo, “Variations in patients’ adherence to medical recommendations: A quantitative review of 50 years of research,” *Med. care*, vol. 42, pp. 200–209, 2004.
- [5] L. G. Heaney and R. Horne, “Non-adherence in difficult asthma: Time to take it seriously,” *Thorax*, vol. 67, no. 3, p. 268–270, 2012.
- [6] G. Kaufman and Y. Birks, “Strategies to improve patients’ adherence to medication,” *Nursing Standard (through 2013)*, vol. 23, no. 49, p. 51, 2009.
- [7] M. R. Sears, D. R. Taylor, C. Print, D. Lake, Q. Li, E. Flannery, D. Yates, M. Lucas, and G. Herbison, “Regular inhaled beta-agonist treatment in bronchial asthma,” *The Lancet*, vol. 336, no. 8728, pp. 1391–1396, 1990.
- [8] M. Asher, S. Montefort, B. Björkstén, C. Lai, D. Strachan, S. Weiland, H. Williams, and I. P. T. S. Group., “Worldwide time trends in the prevalence of symptoms of asthma, allergic rhinoconjunctivitis, and eczema in childhood: Isaac phases one and three repeat multicountry cross-sectional surveys,” *Lancet*, vol. 368, no. 9537, p. 733–743, 2006.
- [9] C. Horn, T. Clark, and G. Cochrane, “Compliance with inhaled therapy and morbidity from asthma,” *Respirat. Med.*, vol. 84, pp. 67–70, 1990.
- [10] L. J. Akinbami, A. E. Simon, and L. M. Rossen, “Changing trends in asthma prevalence among children,” *Pediatrics*, vol. 137, no. 1, p. e20152354, 2016.
- [11] B. T. Association *et al.*, “Death from asthma in two regions of england,” *Br Med J (Clin Res Ed)*, vol. 285, no. 6350, pp. 1251–1255, 1982.
- [12] J. A. Krishnan, K. A. Riekert, J. V. McCoy, D. Y. Stewart, S. Schmidt, A. Chanmugam, P. Hill, and C. S. Rand, “Corticosteroid use after hospital discharge among high-risk adults with asthma,” *American journal of respiratory and critical care medicine*, vol. 170, no. 12, pp. 1281–1285, 2004.
- [13] A. Boutayeb and S. Boutayeb, “The burden of non communicable diseases in developing countries,” *International journal for equity in health*, vol. 4, no. 1, pp. 1–8, 2005.
- [14] R. Fuller, “The diskustm: a new multi-dose powder device—efficacy and comparison with turbuhalertm,” *Journal of aerosol medicine*, vol. 8, no. s2, pp. S–11, 1995.
- [15] L. P. Malmberg, P. Ryttilä, P. Happonen, and T. Haahela, “Inspiratory flows through dry powder inhaler in chronic obstructive pulmonary disease: age and gender rather than severity matters,” *International journal of chronic obstructive pulmonary disease*, vol. 5, p. 257, 2010.
- [16] M. Cavusoglu, M. Kamasak, O. Eroglu, T. Ciloglu, Y. Serinagaoglu, and T. Akcam, “An efficient method for snore/nonsnore classification of sleep sounds,” *Physiological measurement*, vol. 28, no. 8, p. 841, 2007.
- [17] R. C. Sá and Y. Verbandt, “Automated breath detection on long-duration signals using feedforward backpropagation artificial neural networks,” *IEEE transactions on biomedical engineering*, vol. 49, no. 10, pp. 1130–1141, 2002.
- [18] A. Wilson, C. Franks, and I. Freeston, “Algorithms for the detection of breaths from respiratory waveform recordings of infants,” *Medical and Biological Engineering and Computing*, vol. 20, no. 3, pp. 286–292, 1982.
- [19] I. Hossain and Z. Moussavi, “Respiratory airflow estimation by acoustical means,” in *Proceedings of the Second Joint 24th Annual Conference and the Annual Fall Meeting of the Biomedical Engineering Society* [Engineering in Medicine and Biology, vol. 2. IEEE, 2002, pp. 1476–1477.
- [20] S. Huq and Z. Moussavi, “Acoustic breath-phase detection using tracheal breath sounds,” *Medical & biological engineering & computing*, vol. 50, no. 3, pp. 297–308, 2012.
- [21] A. Yadollahi and Z. M. Moussavi, “A robust method for estimating respiratory flow using tracheal sounds entropy,” *IEEE Transactions on Biomedical Engineering*, vol. 53, no. 4, pp. 662–668, 2006.
- [22] A. B and G. J., “Use of pressurized metered dose inhalers in patients with chronic obstructive pulmonary disease: review of evidence,” *Expert review of respiratory medicine*, vol. 8, no. 3, pp. 349–356, 2014.
- [23] S. Howard, A. Lang, M. Patel, S. Sharples, and D. Shaw, “Electronic monitoring of adherence to inhaled medication in asthma,” *Current Respiratory Medicine Reviews*, vol. 10, no. 1, pp. 50–63, 2014.

TABLE V: Experimental evaluation with SVM algorithm
Normalized confusion matrices.

			Multi subject				Single subject				LOSO			
			Drug	Exhale	Inhale	Noise	Drug	Exhale	Inhale	Noise	Drug	Exhale	Inhale	Noise
Spect	Non-mixed	Drug	98.446	0	1.554	0	98.907	0	1.093	0	90	0	10	0
		Exhale	0	98.548	0.806	0.645	0	97.389	1.044	1.567	0	97.468	0.844	1.688
		Inhale	2.508	2.194	95.298	0	3	2.5	94.5	0	2.521	1.681	94.958	0.84
		Noise	0.792	72.277	1.584	25.347	1.153	63.977	1.729	33.141	0	90.506	1.266	8.228
	Mixed	Drug	85.711	2	1.205	11.085	85.588	2.007	1.232	11.173	90.854	0	0	9.146
		Exhale	0.04	98.381	1.052	0.527	0.045	97.342	1.575	1.037	0	97.245	0.552	2.203
		Inhale	4.565	4.301	88.947	2.187	5.577	4.17	87.056	3.197	7.656	4.562	84.68	3.101
		Noise	1.116	92.929	0.745	5.21	1.411	90.771	0.547	7.271	0.884	96.621	0.675	1.821
Cepst	Non-mixed	Drug	94.301	0	3.109	2.591	96.175	0	1.639	2.186	90	0	10	0
		Exhale	0	96.916	0.649	2.435	0	96.042	0.792	3.166	0	67.932	0.422	31.646
		Inhale	0.94	2.194	96.552	0.313	0.5	2.5	97	0	19.328	2.521	72.269	5.882
		Noise	2	4	1	93	2.632	4.971	1.17	91.228	0	0.633	0.633	98.734
	Mixed	Drug	73.196	0.225	1.47	25.109	75.204	0.194	1.481	23.121	58.232	0	0.61	41.159
		Exhale	0.17	91.68	0.441	7.708	0.284	91.6	0.695	7.421	0.039	57.366	0	42.595
		Inhale	5.701	4.18	83.494	6.625	7.053	4.405	84.671	3.87	17.378	5.973	52.148	24.502
		Noise	1.03	4.645	0.548	93.777	1.475	5.411	0.551	92.563	0.452	1.824	0.343	97.381
MFCC	Non-mixed	Drug	97.927	0	1.036	1.036	97.814	0	1.093	1.093	100	0	0	0
		Exhale	0	96.613	0.645	2.742	0	95.822	0.783	3.394	0	65.823	0.422	33.755
		Inhale	1.567	1.881	96.552	0	1.5	2.5	96	0	12.605	1.681	78.992	6.723
		Noise	0.99	3.564	0.99	94.455	1.441	2.882	1.153	94.524	0	1.266	0.633	98.101
	Mixed	Drug	84.876	0.503	0.675	13.945	85.062	0.291	0.651	13.997	78.659	0	0	21.341
		Exhale	0.18	91.739	0.558	7.524	0.284	91.816	0.682	7.218	0	57.748	0	42.252
		Inhale	9.869	3.871	83.772	2.488	9.835	3.907	83.375	2.883	14.262	4.771	69.67	11.297
		Noise	1.482	4.723	0.399	93.397	1.663	4.704	0.341	93.291	1.22	1.916	0.389	96.475

TABLE VI: Experimental evaluation with Random Forest algorithm
Normalized confusion matrices.

			Multi subject				Single subject				LOSO			
			Drug	Exhale	Inhale	Noise	Drug	Exhale	Inhale	Noise	Drug	Exhale	Inhale	Noise
Spect	Non-mixed	Drug	97.927	0	1.554	0.518	98.907	0	0.546	0.546	70	0	30	0
		Exhale	0	92.097	0.806	7.097	0	92.689	0.783	6.527	0	80.591	0.422	18.987
		Inhale	2.194	2.194	94.984	0.627	4.5	2.5	93	0	4.202	1.681	91.597	2.521
		Noise	0.99	7.921	1.188	89.901	1.729	4.899	1.153	92.219	0	13.291	0.633	86.076
	Mixed	Drug	84.399	0.185	1.139	14.276	83.899	0.263	1.094	14.745	89.024	0	0	10.976
		Exhale	0.003	87.343	0.837	11.817	0.003	89.498	1.044	9.455	0	73.445	0	26.555
		Inhale	3.227	2.918	89.928	3.927	4.11	3.358	88.246	4.285	5.087	3.051	83.788	8.074
		Noise	0.928	7.97	0.953	90.149	1.176	7.603	0.748	90.473	0.441	8.208	0.967	90.385
Cepst	Non-mixed	Drug	91.192	1.036	2.591	5.181	93.989	0.546	1.093	4.372	70	0	30	0
		Exhale	0	96.266	0.649	3.084	0	94.987	0.792	4.222	0	86.92	0.422	12.658
		Inhale	1.567	2.194	96.238	0	2	3	95	0	1.681	2.521	94.958	0.84
		Noise	2	6	0.8	91.2	2.924	5.556	0.877	90.643	0	0	0.633	99.367
	Mixed	Drug	62.588	1.139	0.94	35.333	64.35	0.305	0.678	34.667	53.049	0	0	46.951
		Exhale	0.138	92.414	0.547	6.901	0.302	90.53	0.788	8.38	0	77.674	0.13	22.196
		Inhale	2.831	5.467	84.287	7.415	3.432	4.756	84.648	7.164	5.354	5.152	78.549	10.945
		Noise	0.65	5.076	0.464	93.81	0.956	5.063	0.413	93.569	0.124	2.169	0.355	97.351
MFCC	Non-mixed	Drug	95.337	0	2.591	2.073	96.175	0	1.639	2.186	100	0	0	0
		Exhale	0	95.645	0.645	3.71	0.261	94.778	0.783	4.178	0	83.122	0.422	16.456
		Inhale	1.254	2.194	96.552	0	1.5	2.5	96	0	6.723	1.681	91.597	0
		Noise	1.584	4.752	1.188	92.475	2.305	5.764	1.153	90.778	0	1.266	0.633	98.101
	Mixed	Drug	79.221	0.874	1.099	18.805	78.845	0.415	1.121	19.618	75.61	0	0	24.39
		Exhale	0.287	92.831	0.577	6.305	0.579	91.861	0.803	6.757	0	77.071	0	22.929
		Inhale	9.071	4.992	82.108	3.829	10.033	4.881	80.921	4.166	13.989	3.44	75.693	6.879
		Noise	0.989	6.352	0.404	92.255	1.241	5.836	0.342	92.581	0.559	3.323	0.43	95.689

[24] J. Pilcher, M. Holliday, S. Ebmeier, S. McKinstry, F. Messaoudi, M. Weatherall, and R. Beasley, "Validation of a metered dose inhaler electronic monitoring device: implications for asthma clinical trial use," *BMJ open respiratory research*, vol. 3, no. 1, p. e000128, 2016.

[25] M. Holmes, S. D'Arcy, R. Costello, and R. B. Reilly, "Acoustic analysis of inhaler sounds from community-dwelling asthmatic patients for automatic assessment of adherence," *IEEE journal of translational engineering in health and medicine*, vol. 2, pp. 1–10, 2014.

[26] W. M. Hartmann, *Signals, sound, and sensation*. Springer Science & Business Media, 2004.

[27] D. R. Raichel, *The science and applications of acoustics*. Springer Science & Business Media, 2006.

[28] C. B. Bärnes and C. S. Ulrik, "Asthma and adherence to inhaled corticosteroids: current status and future perspectives," *Respiratory care*, vol. 60, no. 3, pp. 455–468, 2015.

[29] S. D'Arcy, E. MacHale, J. Scheult, M. Holmes, C. Hughes, I. Sulaiman, D. Hyland, C. O'Reilly, S. Glynn, T. Al-Zaabi, J. McCourt, T. Taylor, F. Keane, I. Killane, R. Reilly, and R. Costello, "A method to assess adherence in inhaler use through analysis of acoustic recordings of inhaler events,," *PLoS ONE*, vol. 9, no. 6, 2014.

[30] J. N. Pritchard and C. Nicholls, "Emerging technologies for electronic monitoring of adherence, inhaler competence, and true adherence," *J. Aerosol Med. Pulmonary Drug Del.*, vol. 28, no. 2, p. 69–81, 2015.

[31] H. Chrystyn and D. Price, "Not all asthma inhalers are the same: factors to consider when prescribing an inhaler," *Primary Care Respiratory Journal*, vol. 18, no. 4, pp. 243–249, 2009.

[32] R. A. Al-Showair, W. Y. Tarsin, K. H. Assi, S. B. Pearson, and H. Chrystyn, "Can all patients with copd use the correct inhalation flow with all inhalers and does training help?" *Respiratory medicine*, vol. 101, no. 11, pp. 2395–2401, 2007.

[33] W. G. Ammari and H. Chrystyn, "Optimizing the inhalation flow and technique through metered dose inhalers of asthmatic adults and

TABLE VII: Experimental evaluation with Adaboost algorithm
Normalized confusion matrices.

			Multi subject				Single subject				LOSO			
			Drug	Exhale	Inhale	Noise	Drug	Exhale	Inhale	Noise	Drug	Exhale	Inhale	Noise
Spect	Non-mixed	Drug	96.373	0	3.109	0.518	96.721	0	2.732	0.546	70	0	30	0
		Exhale	0	94.194	0.806	5	0	94.517	1.044	4.439	0	78.903	0.422	20.675
		Inhale	1.567	2.194	96.238	0	4	3.5	92.5	0	6.723	1.681	86.555	5.042
	Mixed	Noise	1.188	6.535	0.792	91.485	1.441	8.357	0.576	89.625	0	5.696	0.633	93.671
		Drug	84.399	0.185	0.768	14.647	80.756	0.872	2.284	16.087	89.024	0	0	10.976
		Exhale	0.029	89.81	0.842	9.32	0.211	87.467	1.193	11.128	0	71.282	0	28.718
Cepst	Non-mixed	Inhale	3.362	2.96	90.665	3.013	4.304	4.562	86.23	4.904	9.225	3.49	76.937	10.348
		Noise	0.832	8.314	1.014	89.841	1.025	8.451	0.662	89.862	0.489	7.969	0.896	90.646
		Drug	93.264	0	2.591	4.145	93.443	0	2.186	4.372	70	0	10	20
	Mixed	Exhale	0	96.916	0.649	2.435	0.264	93.668	1.319	4.749	0	89.873	0.422	9.705
		Inhale	0.94	2.194	96.865	0	2	3.5	94	0.5	3.361	1.681	94.958	0
		Noise	2.2	4.8	0.8	92.2	2.632	6.14	1.17	90.058	0.633	0	0.633	98.734
MFCC	Non-mixed	Drug	66.481	0.821	1.099	31.598	67.077	0.997	1.495	30.431	41.768	0	0.305	57.927
		Exhale	0.151	92.149	0.596	7.105	0.77	89.463	1.153	8.614	0	77.745	0	22.255
		Inhale	3.233	5.369	83.862	7.536	5.208	5.402	81.516	7.874	7.009	4.375	77.635	10.981
	Mixed	Noise	0.733	4.585	0.434	94.248	1.17	4.946	0.52	93.364	0.166	2.074	0.318	97.442
		Drug	97.927	0	1.554	0.518	93.989	0.546	2.186	3.279	90	0	0	10
		Exhale	0	96.774	0.645	2.581	0.522	93.473	0.783	5.222	0	85.232	0.422	14.346
MFCC	Non-mixed	Inhale	0.627	2.194	97.179	0	1	3.5	94.5	1	21.849	1.681	74.79	1.681
		Noise	1.584	4.158	0.99	93.267	1.153	3.458	1.729	93.66	0	0.633	0.633	98.734
		Drug	80.93	0.649	0.596	17.825	75.813	1.025	3.101	20.061	69.207	0.305	0	30.488
	Mixed	Exhale	0.224	93.766	0.619	5.391	0.647	88.733	1.585	9.035	0	78.285	0	21.715
		Inhale	7.817	4.551	84.177	3.455	8.603	6.938	79.546	4.913	20.717	3.504	68.986	6.793
		Noise	1.091	5.748	0.43	92.731	1.226	6.753	0.387	91.634	0.542	3.395	0.441	95.622

TABLE VIII: Experimental evaluation with GMM algorithm
Normalized confusion matrices.

			Multi subject				Single subject				LOSO			
			Drug	Exhale	Inhale	Noise	Drug	Exhale	Inhale	Noise	Drug	Exhale	Inhale	Noise
Spect	Non-mixed	Drug	95.337	0	4.145	0.518	96.175	0	3.825	0	40	0	60	0
		Exhale	0.161	84.516	1.613	13.71	0.522	83.29	5.744	10.444	0	77.637	1.266	21.097
		Inhale	1.881	1.254	95.611	1.254	2.5	2.5	95	0	2.521	0	94.118	3.361
	Mixed	Noise	1.188	15.446	2.574	80.792	1.153	15.85	2.882	80.115	0	18.987	0.633	80.38
		Drug	85.803	0.596	2.622	10.979	86.017	1.025	2.658	10.3	72.866	0	16.768	10.366
		Exhale	0.058	74.293	2.308	23.341	0.174	78.715	3.782	17.329	0	63.384	0.792	35.824
Cepst	Non-mixed	Inhale	2.665	2.03	93.079	2.226	3.238	2.357	92.384	2.02	4.13	1.454	86.997	7.419
		Noise	1.141	8.222	1.724	88.912	1.63	8.036	2.089	88.245	0.438	8.371	1.135	90.056
		Drug	95.337	0.518	1.036	3.109	95.628	1.093	0.546	2.732	50	0	20	30
	Mixed	Exhale	0	95.617	0.649	3.734	0	95.251	0.792	3.958	0	80.169	0.422	19.409
		Inhale	0.94	2.194	95.925	0.94	1	2.5	96	0.5	0.84	1.681	60.504	36.975
		Noise	3	5.6	0.8	90.6	2.632	5.556	1.17	90.643	0	0.633	0	99.367
MFCC	Non-mixed	Drug	72.984	1.192	0.755	25.07	72.172	1.703	0.761	25.363	42.683	0	0	57.317
		Exhale	0.108	90.183	0.516	9.194	0.176	87.908	0.617	11.3	0	64.026	0	35.974
		Inhale	5.633	5.518	75.486	13.363	5.231	7.801	76.566	10.402	3.706	2.957	32.007	61.33
	Mixed	Noise	0.923	6.326	0.245	92.505	1.172	6.294	0.247	92.287	0.141	3.921	0.104	95.834
		Drug	5.699	41.969	33.679	18.653	10.929	46.448	30.601	12.022	0	70	0	30
		Exhale	0	99.355	0.323	0.323	0.522	98.172	0.522	0.783	0	96.203	0.422	3.376
MFCC	Non-mixed	Inhale	0	30.721	60.815	8.464	0	14.5	85	0.5	1.681	66.387	31.933	0
		Noise	0	13.663	0.99	85.347	3.458	33.141	5.764	57.637	0.633	4.43	0	94.937
		Drug	11.018	32.592	16.74	39.65	0.235	50.422	32.812	16.531	0	60.061	0	39.939
	Mixed	Exhale	0	97.04	0.27	2.689	0	97.146	0.566	2.288	0	94.451	0	5.549
		Inhale	2.715	40.281	39.334	17.67	0	50.867	47.214	1.919	3.476	65.662	26.545	4.317
		Noise	0.161	11.463	0.418	87.958	0	15.754	2.508	81.738	0.18	10.78	0.195	88.846

TABLE IX: Experimental evaluation with LSTM RNNs
Normalized confusion matrices.

			Multi subject				Single subject				LOSO			
			Drug	Exhale	Inhale	Noise	Drug	Exhale	Inhale	Noise	Drug	Exhale	Inhale	Noise
Spect	Non-mixed	Drug	99.085	0.076	0.153	0.686	98.808	0.159	0.556	0.477	100	0	0	0
		Exhale	0.036	96.483	0.58	2.901	0.235	94.975	0.823	3.967	0	88.027	0.473	11.5
		Inhale	0.07	2.369	97.353	0.209	0	0.944	98.889	0.167	1.214	7.003	88.422	3.361
	Mixed	Noise	0.276	3.259	0.501	95.964	0.139	3.555	0.627	95.678	0.179	1.875	0.804	97.143
		Drug	82.047	0.465	0.744	16.744	82.056	0.582	0.582	16.78	90.909	0	0	9.091
		Exhale	0.05	89.562	0.825	9.562	0.098	90.085	0.837	8.979	0.026	79.261	0.104	20.609
Mixed	Inhale	2.91	3.246	91.959	1.884	3.583	4.257	89.832	2.328	2.387	9.165	82.53	5.919	
	Noise	1.027	3.913	1.016	94.045	1.07	4.605	0.963	93.362	1.128	2.728	0.716	95.428	

TABLE X: Experimental evaluation with CNNs
Normalized confusion matrices.

		Multi subject				Single subject				LOSO				
		Drug	Exhale	Inhale	Noise	Drug	Exhale	Inhale	Noise	Drug	Exhale	Inhale	Noise	
Time	Non-mixed	Drug	83.753	1.292	1.156	13.8	88.061	0.069	0.828	11.042	63.636	0	0	36.364
		Exhale	0.043	96.537	1.425	1.995	0.002	92.264	1.565	6.168	0	91.826	0.43	7.745
		Inhale	0.048	2.637	97.19	0.124	0.058	3.427	96.322	0.193	0	1.727	98.066	0.207
		Noise	0.974	9.475	2.147	87.404	1.24	8.468	1.427	88.865	0.116	0.581	4.355	94.948
	Mixed	Drug	65.316	0.662	1.086	32.936	65.056	0.471	3.143	31.33	66.768	0.305	0	32.927
		Exhale	0.098	88.828	0.892	10.181	0.131	83.73	1.596	14.543	0	86.707	0	13.293
		Inhale	3.646	4.599	85.85	5.906	3.229	4.802	87.789	4.179	1.403	1.785	93.481	3.332
		Noise	1.379	3.791	0.495	94.335	1.386	3.895	0.758	93.961	1.746	2.452	0.664	95.138

TABLE XI: Experimental evaluation with SVM algorithm
Non-normalized confusion matrices.

		Multi subject				Single subject				LOSO				
		Drug	Exhale	Inhale	Noise	Drug	Exhale	Inhale	Noise	Drug	Exhale	Inhale	Noise	
Spect	Non-mixed	Drug	190	0	3	0	181	0	2	0	9	0	1	0
		Exhale	0	611	5	4	0	373	4	6	0	231	2	4
		Inhale	8	7	304	0	6	5	189	0	3	2	113	1
		Noise	4	365	8	128	4	222	6	115	0	143	2	13
	Mixed	Drug	6472	151	91	837	6182	145	89	807	298	0	0	30
		Exhale	26	64056	685	343	18	38680	626	412	0	24675	140	559
		Inhale	1624	1530	31643	778	1209	904	18872	693	1064	634	11768	431
		Noise	2535	211064	1692	11832	2184	140515	846	11256	639	69878	488	1317
Cepst	Non-mixed	Drug	182	0	6	5	176	0	3	4	9	0	1	0
		Exhale	0	597	4	15	0	364	3	12	0	161	1	75
		Inhale	3	7	308	1	1	5	194	0	23	3	86	7
		Noise	10	20	5	465	9	17	4	312	0	1	1	156
	Mixed	Drug	5527	17	111	1896	5432	14	107	1670	191	0	2	135
		Exhale	111	59693	287	5019	113	36398	276	2949	10	14556	0	10808
		Inhale	2028	1487	29703	2357	1529	955	18355	839	2415	830	7247	3405
		Noise	2339	10549	1245	212990	2283	8377	853	143288	327	1319	248	70428
MFCC	Non-mixed	Drug	189	0	2	2	179	0	2	2	10	0	0	0
		Exhale	0	599	4	17	0	367	3	13	0	156	1	80
		Inhale	5	6	308	0	3	5	192	0	15	2	94	8
		Noise	5	18	5	477	5	10	4	328	0	2	1	155
	Mixed	Drug	6409	38	51	1053	6144	21	47	1011	258	0	0	70
		Exhale	117	59731	363	4899	113	36484	271	2868	0	14653	0	10721
		Inhale	3511	1377	29802	885	2132	847	18074	625	1982	663	9682	1570
		Noise	3365	10726	907	212125	2575	7282	528	144416	882	1386	281	69773

TABLE XII: Experimental evaluation with Random Forest algorithm
Non-normalized confusion matrices.

		Multi subject				Single subject				LOSO				
		Drug	Exhale	Inhale	Noise	Drug	Exhale	Inhale	Noise	Drug	Exhale	Inhale	Noise	
Spect	Non-mixed	Drug	189	0	3	1	181	0	1	1	7	0	3	0
		Exhale	0	571	5	44	0	355	3	25	0	191	1	45
		Inhale	7	7	303	2	9	5	186	0	5	2	109	3
		Noise	5	40	6	454	6	17	4	320	0	21	1	136
	Mixed	Drug	6373	14	86	1078	6060	19	79	1065	292	0	0	36
		Exhale	2	56869	545	7694	1	35563	415	3757	0	18636	0	6738
		Inhale	1148	1038	31992	1397	891	728	19130	929	707	424	11644	1122
		Noise	2108	18101	2165	204749	1820	11770	1158	140053	319	5936	699	65368
Cepst	Non-mixed	Drug	176	2	5	10	172	1	2	8	7	0	3	0
		Exhale	0	593	4	19	0	360	3	16	0	206	1	30
		Inhale	5	7	307	0	4	6	190	0	2	3	113	1
		Noise	10	30	4	456	10	19	3	310	0	0	1	157
	Mixed	Drug	4726	86	71	2668	4648	22	49	2504	174	0	0	154
		Exhale	90	60171	356	4493	120	35973	313	3330	0	19709	33	5632
		Inhale	1007	1945	29985	2638	744	1031	18350	1553	744	716	10916	1521
		Noise	1477	11529	1053	213064	1480	7837	639	144845	90	1569	257	70406
MFCC	Non-mixed	Drug	184	0	5	4	176	0	3	4	10	0	0	0
		Exhale	0	593	4	23	1	363	3	16	0	197	1	39
		Inhale	4	7	308	0	3	5	192	0	8	2	109	0
		Noise	8	24	6	467	8	20	4	315	0	2	1	155
	Mixed	Drug	5982	66	83	1420	5695	30	81	1417	248	0	0	80
		Exhale	187	60442	376	4105	230	36502	319	2685	0	19556	0	5818
		Inhale	3227	1776	29210	1362	2175	1058	17542	903	1944	478	10519	956
		Noise	2246	14427	918	209532	1921	9034	529	143317	404	2403	311	69204

TABLE XIII: Experimental evaluation with Adaboost algorithm
Non-normalized confusion matrices.

		Multi subject				Single subject				LOSO				
		Drug	Exhale	Inhale	Noise	Drug	Exhale	Inhale	Noise	Drug	Exhale	Inhale	Noise	
Spect	Non-mixed	Drug	186	0	6	1	177	0	5	1	7	0	3	0
		Exhale	0	584	5	31	0	362	4	17	0	187	1	49
		Inhale	5	7	307	0	8	7	185	0	8	2	103	6
		Noise	6	33	4	462	5	29	2	311	0	9	1	148
	Mixed	Drug	6373	14	58	1106	5833	63	165	1162	292	0	0	36
		Exhale	19	58475	548	6068	84	34756	474	4422	0	18087	0	7287
		Inhale	1196	1053	32254	1072	933	989	18693	1063	1282	485	10692	1438
	Noise	1890	18882	2302	204049	1586	13083	1025	139107	354	5763	648	65557	
Cepst	Non-mixed	Drug	180	0	5	8	171	0	4	8	7	0	1	2
		Exhale	0	597	4	15	1	355	5	18	0	213	1	23
		Inhale	3	7	309	0	4	7	188	1	4	2	113	0
		Noise	11	24	4	461	9	21	4	308	1	0	1	156
	Mixed	Drug	5020	62	83	2386	4845	72	108	2198	137	0	1	190
		Exhale	98	59998	388	4626	306	35549	458	3423	0	19727	0	5647
		Inhale	1150	1910	29834	2681	1129	1171	17671	1707	974	608	10789	1526
Noise		1665	10414	985	214059	1811	7657	805	144528	120	1500	230	70472	
MFCC	Non-mixed	Drug	189	0	3	1	172	1	4	6	9	0	0	1
		Exhale	0	600	4	16	2	358	3	20	0	202	1	34
		Inhale	2	7	310	0	2	7	189	2	26	2	89	2
		Noise	8	21	5	471	4	12	6	325	0	1	1	156
	Mixed	Drug	6111	49	45	1346	5476	74	224	1449	227	1	0	100
		Exhale	146	61051	403	3510	257	35259	630	3590	0	19864	0	5510
		Inhale	2781	1619	29946	1229	1865	1504	17244	1065	2879	487	9587	944
Noise		2478	13054	977	210614	1898	10454	599	141850	392	2455	319	69156	

TABLE XIV: Experimental evaluation with GMM based algorithm
Non-normalized confusion matrices.

		Multi subject				Single subject				LOSO				
		Drug	Exhale	Inhale	Noise	Drug	Exhale	Inhale	Noise	Drug	Exhale	Inhale	Noise	
Spect	Non-mixed	Drug	184	0	8	1	176	0	7	0	4	0	6	0
		Exhale	1	524	10	85	2	319	22	40	0	184	3	50
		Inhale	6	4	305	4	5	5	190	0	3	0	112	4
		Noise	6	78	13	408	4	55	10	278	0	30	1	127
	Mixed	Drug	6479	45	198	829	6213	74	192	744	239	0	55	34
		Exhale	38	48372	1503	15197	69	31278	1503	6886	0	16083	201	9090
		Inhale	948	722	33113	792	702	511	20027	438	574	202	12090	1031
	Noise	2592	18675	3916	201940	2523	12440	3234	136604	317	6054	821	65130	
Cepst	Non-mixed	Drug	184	1	2	6	175	2	1	5	5	0	2	3
		Exhale	0	589	4	23	0	361	3	15	0	190	1	46
		Inhale	3	7	306	3	2	5	192	1	1	2	72	44
		Noise	15	28	4	453	9	19	4	310	0	1	0	157
	Mixed	Drug	5511	90	57	1893	5213	123	55	1832	140	0	0	188
		Exhale	70	58718	336	5986	70	34931	245	4490	0	16246	0	9128
		Inhale	2004	1963	26854	4754	1134	1691	16598	2255	515	411	4448	8523
Noise		2097	14368	557	210101	1815	9743	382	142861	102	2836	75	69309	
MFCC	Non-mixed	Drug	11	81	65	36	20	85	56	22	0	7	0	3
		Exhale	0	616	2	2	2	376	2	3	0	228	1	8
		Inhale	0	98	194	27	0	29	170	1	2	79	38	0
		Noise	0	69	5	431	12	115	20	200	1	7	0	150
	Mixed	Drug	832	2461	1264	2994	17	3642	2370	1194	0	197	0	131
		Exhale	0	63183	176	1751	0	38602	225	909	0	23966	0	1408
		Inhale	966	14330	13993	6286	0	11027	10235	416	483	9125	3689	600
Noise		365	26035	950	199773	0	24388	3882	126531	130	7796	141	64255	

TABLE XV: Experimental evaluation with LSTM RNNs
Non-normalized confusion matrices.

		Multi subject				Single subject				LOSO				
		Drug	Exhale	Inhale	Noise	Drug	Exhale	Inhale	Noise	Drug	Exhale	Inhale	Noise	
Spect	Non-mixed	Drug	1299	1	2	9	1243	2	7	6	53	0	0	0
		Exhale	2	5322	32	160	8	3232	28	135	0	1860	10	243
		Inhale	2	68	2795	6	0	17	1780	3	13	75	947	36
		Noise	11	130	20	3828	4	102	18	2745	2	21	9	1088
	Mixed	Drug	882	5	8	180	846	6	6	173	40	0	0	4
		Exhale	5	8898	82	950	6	5488	51	547	1	3046	4	792
		Inhale	156	174	4929	101	117	139	2933	76	50	192	1729	124
	Noise	381	1452	377	34901	270	1162	243	23559	134	324	85	11334	

TABLE XVI: Experimental evaluation with CNNs
Non-normalized confusion matrices.

		Multi subject				Single subject				LOSO				
		Drug	Exhale	Inhale	Noise	Drug	Exhale	Inhale	Noise	Drug	Exhale	Inhale	Noise	
Time	Non-mixed	Drug	1232	19	17	203	1276	1	12	160	14	0	0	8
		Exhale	36	80906	1194	1672	1	47268	802	3160	0	29914	140	2523
		Inhale	22	1209	44554	57	16	942	26480	53	0	317	17996	38
		Noise	215	2092	474	19298	231	1578	266	16560	4	20	150	3270
	Mixed	Drug	4932	50	82	2487	4699	34	227	2263	219	1	0	108
		Exhale	64	57836	581	6629	52	33271	634	5779	0	22001	0	3373
		Inhale	1297	1636	30541	2101	700	1041	19031	906	195	248	12991	463
		Noise	3133	8610	1124	214256	2146	6030	1173	145452	1263	1773	480	68806

children attending a community pharmacy," *Journal of Asthma*, vol. 50, no. 5, pp. 505–513, 2013.

[34] I. Sulaiman, B. Cushen, G. Greene, J. Seheult, D. Seow, F. Rawat, E. MacHale, M. Mokoka, C. N. Moran, A. Sartini Bhreathnach *et al.*, "Objective assessment of adherence to inhalers by patients with chronic obstructive pulmonary disease," *American journal of respiratory and critical care medicine*, vol. 195, no. 10, pp. 1333–1343, 2017.

[35] M. W. Sims, "Aerosol therapy for obstructive lung diseases: device selection and practice management issues," *Chest*, vol. 140, no. 3, pp. 781–788, 2011.

[36] J. N. Seheult, P. O'Connell, K. C. Tee, T. Bholah, H. Al Bannai, I. Sulaiman, E. MacHale, S. D'Arcy, M. S. Holmes, D. Bergin *et al.*, "The acoustic features of inhalation can be used to quantify aerosol delivery from a diskus™ dry powder inhaler," *Pharmaceutical research*, vol. 31, no. 10, pp. 2735–2747, 2014.

[37] M. J. Crocker, *Encyclopedia of acoustics*. Wiley-Interscience, 1997, vol. 3.

[38] M. Masoli, D. Fabian, S. Holt, R. Beasley, and G. I. for Asthma (GINA) Program, "The global burden of asthma: executive summary of the gina dissemination committee report," *Allergy*, vol. 59, no. 5, pp. 469–478, 2004.

[39] S. J. Farr, A. M. Rowe, R. Rubsamem, and G. Taylor, "Aerosol deposition in the human lung following administration from a microprocessor controlled pressurised metered dose inhaler," *Thorax*, vol. 50, no. 6, pp. 639–644, 1995.

[40] S. Warren, S. Farr, G. Taylor, P. Lloyd, J. Okikawa, J. Schuster, A. Rowe, and R. Rubsamem, "Comparison of aerosol deposition from a solution mdi and a novel liquid aerosol generator in healthy volunteers," *European Journal of Pharmaceutical Sciences*, no. 4, p. S141, 1996.

[41] J. L. Rau, "Determinants of patient adherence to an aerosol regimen," *Respiratory care*, vol. 50, no. 10, pp. 1346–1359, 2005.

[42] D. Bogen and A. J. Apter, "Adherence logger for a dry powder inhaler: a new device for medical adherence research," *Journal of allergy and clinical immunology*, vol. 114, no. 4, pp. 863–868, 2004.

[43] D. Bogen and A. Apter, "The reliability of the diskus adherence logger (dal)," *Journal of Allergy and Clinical Immunology*, vol. 115, no. 2, p. S42, 2005.

[44] J. M. Foster, L. Smith, T. Usherwood, S. M. Sawyer, C. S. Rand, and H. K. Reddel, "The reliability and patient acceptability of the smarttrack device: a new electronic monitor and reminder device for metered dose inhalers," *Journal of Asthma*, vol. 49, no. 6, pp. 657–662, 2012.

[45] A. H. Y. Chan, A. W. Stewart, J. Harrison, P. N. Black, E. A. Mitchell, and J. M. Foster, "Electronic adherence monitoring device performance and patient acceptability: a randomized control trial," *Expert review of medical devices*, vol. 14, no. 5, pp. 401–411, 2017.

[46] L. Gradinarsky and T. Löf, "Inhalation adherence monitoring using smart electronic add-on device: Accuracy evaluation using simulated real-life test program," in *2014 4th International Conference on Wireless Mobile Communication and Healthcare-Transforming Healthcare Through Innovations in Mobile and Wireless Technologies (MOBI-HEALTH)*. IEEE, 2014, pp. 145–147.

[47] J. Pilcher, P. Shirtcliffe, M. Patel, S. McKinstry, T. Cripps, M. Weatherall, and R. Beasley, "Three-month validation of a turbuhaler electronic monitoring device: implications for asthma clinical trial use," *BMJ open respiratory research*, vol. 2, no. 1, p. e000097, 2015.

[48] S. D'Arcy, E. MacHale, J. Seheult, M. S. Holmes, C. Hughes, I. Sulaiman, D. Hyland, C. O'Reilly, S. Glynn, T. Al-Zaabi *et al.*, "A method to assess adherence in inhaler use through analysis of acoustic recordings of inhaler events," *PLoS one*, vol. 9, no. 6, 2014.

[49] D. Van Sickle, S. Magzamen, S. Truelove, and T. Morrison, "Remote monitoring of inhaled bronchodilator use and weekly feedback about asthma management: an open-group, short-term pilot study of the impact on asthma control," *PLoS One*, vol. 8, no. 2, 2013.

[50] D. Aldridge, "Project red and asthmapolis," *CIN: Computers, Informatics, Nursing*, vol. 29, no. 10, pp. 542–543, 2011.

[51] D. Van Sickle, M. J. Maenner, M. Barrett, and J. E. Marcus, "Monitoring and improving compliance and asthma control: mapping inhaler use for feedback to patients, physicians and payers," *Resp Drug Delivery Europe*, vol. 1, pp. 119–130, 2013.

[52] Pettas, D., Nousias, S., Zacharaki, E. & Moustakas, K. Recognition of breathing activity and medication adherence using lstm neural networks. *2019 IEEE 19th International Conference On Bioinformatics And Bioengineering (BIBE)*. pp. 941-946 (2019)

[53] A. Shakshuki and R. U. Agu, "Improving the efficiency of respiratory drug delivery: a review of current treatment trends and future strategies for asthma and chronic obstructive pulmonary disease," *Pulmonary Therapy*, vol. 3, no. 2, pp. 267–281, 2017.

[54] J. Denyer, "Adherence monitoring in drug delivery," *Expert opinion on drug delivery*, vol. 7, no. 10, pp. 1127–1131, 2010.

[55] S. Nousias, J. Lakoumentas, A. Lalos, D. Kikidis, K. Moustakas, K. Votis, and D. Tzovaras, "Monitoring asthma medication adherence through content based audio classification," in *2016 IEEE Symposium Series on Computational Intelligence (SSCI)*. IEEE, 2016, pp. 1–5.

[56] N. Q. Duong and H.-T. Duong, "A review of audio features and statistical models exploited for voice pattern design," *arXiv preprint arXiv:1502.06811*, 2015.

[57] T. Zhang and C.-C. J. Kuo, "Hierarchical system for content-based audio classification and retrieval," in *Multimedia Storage and Archiving Systems III*, vol. 3527. International Society for Optics and Photonics, 1998, pp. 398–409.

[58] H. Heryanto, S. Akbar, and B. Sitohang, "Direct access in content-based audio information retrieval: A state of the art and challenges," in *Proceedings of the 2011 International Conference on Electrical Engineering and Informatics*. IEEE, 2011, pp. 1–6.

[59] F. Gouyon, F. Pachet, O. Delerue *et al.*, "On the use of zero-crossing rate for an application of classification of percussive sounds," in *Proceedings of the COST G-6 conference on Digital Audio Effects (DAFX-00)*, Verona, Italy, vol. 5. Citeseer, 2000, p. 16.

[60] R. Bachu, S. Kopparthi, B. Adapa, and B. D. Barkana, "Voiced/unvoiced decision for speech signals based on zero-crossing rate and energy," in *Advanced techniques in computing sciences and software engineering*. Springer, 2010, pp. 279–282.

[61] R. Bachu, S. Kopparthi, B. Adapa, and B. Barkana, "Separation of voiced and unvoiced using zero crossing rate and energy of the speech signal," in *American Society for Engineering Education (ASEE) Zone Conference Proceedings*, 2008, pp. 1–7.

[62] D. Shete, S. Patil, and S. Patil, "Zero crossing rate and energy of the speech signal of devanagari script," *IOSR-JVSP*, vol. 4, no. 1, pp. 1–5, 2014.

[63] B. Sharma and P. P. Talukdar, "Zero crossing rate of the voice and unvoiced speech signal of assamese words," *International Journal of Scientific & Engineering Research*, vol. 7, 2016.

[64] B. Bogert, M. Healy, and J. Tukey, "The quefrency analysis of time series for echoes: Cepstrum, pseudo-autocovariance, cross-cepstrum, and saphe cracking," in *Proc. of the Symp. on Time Series Analysis*, pp. 209–243, 1963.

[65] A. V. Oppenheim and R. W. Schaffer, "From frequency to quefrency: A history of the cepstrum," *IEEE Signal Processing Magazine*, p. 95 – 106, 2004.

- [66] R. B. Randall, "A history of cepstrum analysis and its application to mechanical problems," *Mechanical Systems and Signal Processing*, vol. 97, pp. 3–19, 2017.
- [67] G. B. Janvale, R. R. Deshmukh, and S. Gambhire, "Speech feature extraction using mel-frequency cepstral coefficient (mfcc)," *Conference: the Emerging Trends in Computer Science, Communication and Information Technology At: Yaswant Mahavidyalaya, Nanded*, 2010.
- [68] T. Kinnunen and H. Li, "Spectral features for automatic text independent speaker recognition," *Ph.D. thesis, University of Joensuu*, 2010.
- [69] D. Ruinskiy and Y. Lavner, "An effective algorithm for automatic detection and exact demarcation of breath sounds in speech and song signals," *IEEE Trans. Audio, Speech, Lang. Process.*, vol. 15, no. 3, p. 838–850, 2007.
- [70] M. Sahidullah and G. Saha, "Design, analysis and experimental evaluation of block based transformation in mfcc computation for speaker recognition," *Speech communication*, vol. 54, no. 4, pp. 543–565, 2012.
- [71] J. Saini and R. Mehra, "Power spectral density analysis of speech signal using window techniques," *International Journal of Computer Applications*, vol. 131, no. 14, pp. 33–36, 2015.
- [72] A. Nasser, A. Mansour, K. C. Yao, H. Abdallah, and H. Charara, "Spectrum sensing based on cumulative power spectral density," *EURASIP Journal on Advances in Signal Processing*, 2017.
- [73] S. Molau, M. Pitz, R. Schluter, and H. Ney, "Computing mel-frequency cepstral coefficients on the power spectrum," *ICASSP*, 2001.
- [74] F. Zheng, G. Zhang, and Z. Song, "Comparison of different implementations of mfcc," *Journal of Computer science and Technology*, vol. 16, no. 6, pp. 582–589, 2001.
- [75] V. Tyagi and C. Wellekens, "On desensitizing the mel-cepstrum to spurious spectral components for robust speech recognition," in *Proceedings (ICASSP'05). IEEE International Conference on Acoustics, Speech, and Signal Processing, 2005.*, vol. 1. IEEE, 2005, pp. I–529.
- [76] C. Ittichaichareon, S. Suksri, and T. Yingthawornsuk, "Speech recognition using mfcc," *International Conference on Computer Graphics, Simulation and Modeling (ICGSM'2012)*, 2012.
- [77] R. Büssow, "An algorithm for the continuous morlet wavelet transform," *Mechanical Systems and Signal Processing*, vol. 21, no. 8, pp. 2970–2979, 2007.
- [78] V. K. Reddy, K. K. Siramaju, and P. Sircar, "Object detection by 2-d continuous wavelet transform," in *2014 International Conference on Computational Science and Computational Intelligence*, vol. 1. IEEE, 2014, pp. 162–167.
- [79] I. W. Selesnick, R. G. Baraniuk, and N. C. Kingsbury, "The dual-tree complex wavelet transform," *IEEE signal processing magazine*, vol. 22, no. 6, pp. 123–151, 2005.
- [80] D. J. McFarland, C. W. Anderson, K.-R. Muller, A. Schlogl, and D. J. Krusienski, "Bci meeting 2005-workshop on bci signal processing: feature extraction and translation," *IEEE transactions on neural systems and rehabilitation engineering*, vol. 14, no. 2, pp. 135–138, 2006.
- [81] T. Taylor, M. Holmes, I. Sulaiman, S. D'Arcy, R. Costello, and R. Reilly, "An acoustic method to automatically detect pressurized metered dose inhaler actuations," in *2014 36th Annual International Conference of the IEEE Engineering in Medicine and Biology Society*. IEEE, 2014, pp. 4611–4614.
- [82] G. Bradshaw and T. A. Spies, "Characterizing canopy gap structure in forests using wavelet analysis," *Journal of ecology*, pp. 205–215, 1992.
- [83] T. Taylor, Y. Zigel, C. Egan, F. Hughes, R. Costello, and R. Reilly, "Objective assessment of patient inhaler user technique using an audio-based classification approach," *Scientific reports*, vol. 8, no. 1, p. 2164, 2018.
- [84] B. Schölkopf, A. J. Smola, F. Bach *et al.*, *Learning with kernels: support vector machines, regularization, optimization, and beyond*. MIT press, 2002.
- [85] V. Vapnik, "The support vector method of function estimation," in *Nonlinear modeling*. Springer, 1998, pp. 55–85.
- [86] M. Zakariah, "Classification of large datasets using random forest algorithm in various applications: Survey," *International Journal of Engineering and Innovative Technology (IJEIT)*, vol. 4, no. 3, 2014.
- [87] Y. Freund, R. Schapire, and N. Abe, "A short introduction to boosting," *Journal-Japanese Society For Artificial Intelligence*, vol. 14, no. 771–780, p. 1612, 1999.
- [88] T. Hastie, S. Rosset, J. Zhu, and H. Zou, "Multi-class adaboost," *Statistics and its Interface*, vol. 2, no. 3, pp. 349–360, 2009.
- [89] Y. Freund and R. E. Schapire, "A decision-theoretic generalization of on-line learning and an application to boosting," *Journal of computer and system sciences*, vol. 55, no. 1, pp. 119–139, 1997.
- [90] R. E. Schapire, "Using output codes to boost multiclass learning problems," in *ICML*, vol. 97. Citeseer, 1997, pp. 313–321.
- [91] R. E. Schapire and Y. Singer, "Improved boosting algorithms using confidence-rated predictions," *Machine learning*, vol. 37, no. 3, pp. 297–336, 1999.
- [92] E. L. Allwein, R. E. Schapire, and Y. Singer, "Reducing multiclass to binary: A unifying approach for margin classifiers," *Journal of machine learning research*, vol. 1, no. Dec, pp. 113–141, 2000.
- [93] J. Friedman, T. Hastie, and R. Tibshirani, "Additive logistic regression: a statistical view of boosting (with discussion and a rejoinder by the authors)," *The annals of statistics*, vol. 28, no. 2, pp. 337–407, 2000.
- [94] J. H. Friedman, "Greedy function approximation: a gradient boosting machine," *Annals of statistics*, pp. 1189–1232, 2001.
- [95] T. Chengsheng, L. Huacheng, and X. Bing, "Adaboost typical algorithm and its application research," in *MATEC Web of Conferences*, vol. 139. EDP Sciences, 2017, p. 00222.
- [96] S. Nousias, A. S. Lalos, G. Arvanitis, K. Moustakas, T. Tsiarelis, D. Kikidis, K. Votis, and D. Tzovaras, "An mhealth system for monitoring medication adherence in obstructive respiratory diseases using content based audio classification," *IEEE Access, Recent Computational Methods in Knowledge Engineering and Intelligence Computation*, vol. 6, pp. 11 871–11 882, 2018.
- [97] O. Geman, "Nonlinear dynamics, artificial neural networks and neuro-fuzzy classifier for automatic assessing of tremor severity," in *2013 E-Health and Bioengineering Conference (EHB)*. IEEE, 2013, pp. 1–4.
- [98] S. Kiranyaz, T. Ince, and M. Gabbouj, "Real-time patient-specific eeg classification by 1-d convolutional neural networks," *IEEE Transactions on Biomedical Engineering*, vol. 63, no. 3, pp. 664–675, 2015.
- [99] H. Lee, P. Pham, Y. Largman, and A. Ng, "Unsupervised feature learning for audio classification using convolutional deep belief networks," *Advances in neural information processing systems*, vol. 22, pp. 1096–1104, 2009.
- [100] O. Abdel-Hamid, A.-r. Mohamed, H. Jiang, and G. Penn, "Applying convolutional neural networks concepts to hybrid nn-hmm model for speech recognition," in *2012 IEEE international conference on Acoustics, speech and signal processing (ICASSP)*. IEEE, 2012, pp. 4277–4280.
- [101] S. Ji, W. Xu, M. Yang, and K. Yu, "3d convolutional neural networks for human action recognition," *IEEE transactions on pattern analysis and machine intelligence*, vol. 35, no. 1, pp. 221–231, 2012.
- [102] M. S. Hussain and M. A. Haque, "Swishnet: A fast convolutional neural network for speech, music and noise classification and segmentation," *Published in ArXiv*, 2018.
- [103] O. Köpklü, A. Gunduz, N. Kose, and G. Rigoll, "Real-time hand gesture detection and classification using convolutional neural networks," *arXiv preprint arXiv:1901.10323*, 2019.
- [104] Krizhevsky, Alex, Sutskever, Ilya, Hinton, and G. E., "Imagenet classification with deep convolutional neural networks," in *Advances in neural information processing systems*, 2012, pp. 1097–1105.
- [105] D. Kikidis, K. Votis, and D. Tzovaras, "Utilizing convolution neural networks for the acoustic detection of inhaler actuations," in *E-Health and Bioengineering Conference (EHB), 2015*. IEEE, 2015, pp. 1–4.
- [106] V. Ntalianis, S. Nousias, A. S. Lalos, M. Birbas, N. Tsafas, and K. Moustakas, "Assessment of medication adherence in respiratory diseases through deep sparse convolutional coding," in *2019 24th IEEE International Conference on Emerging Technologies and Factory Automation (ETFA)*. IEEE, 2019, pp. 1657–1660.
- [107] V. Ntalianis, N. D. Fakotakis, S. Nousias, A. S. Lalos, M. Birbas, E. I. Zacharaki, and K. Moustakas, "Deep cnn sparse coding for real time inhaler sounds classification," *Sensors*, vol. 20, no. 8, p. 2363, 2020.
- [108] H. Wu and X. Gu, "Max-pooling dropout for regularization of convolutional neural networks," in *International Conference on Neural Information Processing*. Springer, 2015, pp. 46–54.
- [109] D. Pettas, S. Nousias, E. I. Zacharaki, and K. Moustakas, "Recognition of breathing activity and medication adherence using lstm neural networks," *2019 IEEE 19th International Conference on Bioinformatics and Bioengineering (BIBE)*, 2019.
- [110] N. Srivastava, G. Hinton, A. Krizhevsky, I. Sutskever, and R. Salakhutdinov, "Dropout: a simple way to prevent neural networks from overfitting," *The journal of machine learning research*, vol. 15, no. 1, pp. 1929–1958, 2014.
- [111] L. Liu and H. Qi, "Learning effective binary descriptors via cross entropy," in *2017 IEEE Winter Conference on Applications of Computer Vision (WACV)*. IEEE, 2017, pp. 1251–1258.
- [112] D. P. Kingma and J. Ba, "Adam: A method for stochastic optimization," *arXiv preprint arXiv:1412.6980*, 2014.

- [113] R. Horne, J. Weinman, N. Barber, R. Elliott, M. Morgan, A. Cribb, and I. Kellar, "Concordance, adherence and compliance in medicine taking," *London: NCCSDO*, vol. 2005, pp. 40–6, 2005.
- [114] B. Bender, H. Milgrom, and C. Rand, "Nonadherence in asthmatic patients: is there a solution to the problem?" *Annals of Allergy, Asthma & Immunology*, vol. 79, no. 3, pp. 177–187, 1997.
- [115] A. Murphy, A. Proeschal, C. Brightling, A. Wardlaw, I. Pavord, P. Bradding, and R. Green, "The relationship between clinical outcomes and medication adherence in difficult-to-control asthma," *Thorax*, pp. thoraxjnl–2011, 2012.
- [116] J. Oprehek, P. Gayard, C. Grimaud, and J. Charpin, "Patient error in use of bronchodilator metered aerosols." *British medical journal*, vol. 1, no. 6001, p. 76, 1976.
- [117] I. Paterson and G. Crompton, "Use of pressurised aerosols by asthmatic patients." *British medical journal*, vol. 1, no. 6001, p. 76, 1976.
- [118] E. Hesselink, B. W. Penninx, H. A. Wijnhoven, D. M. Kriegsman, J. T. van Eijk, and Arlette, "Determinants of an incorrect inhalation technique in patients with asthma or copd." *Scandinavian journal of primary health care*, vol. 19, no. 4, pp. 255–260, 2001.
- [119] A. Melani, M. Bonavia, V. Cilenti, C. Cinti, P. M. M. Lodi, M. Serra, N. Scichilone, P. Sestini, M. Aliani, and M. Neri, "Inhaler mishandling remains common in real life and is associated with reduced disease control," *Respir Med.*, p. 930–938, 2011.
- [120] J. Dhanani, J. F. Fraser, H.-K. Chan, J. Rello, J. Cohen, and J. A. Roberts, "Fundamentals of aerosol therapy in critical care," *Critical Care*, vol. 20, no. 1, pp. 1–16, 2016.
- [121] M. Farge, "Wavelet transforms and their applications to turbulence," *Annual review of fluid mechanics*, vol. 24, no. 1, pp. 395–458, 1992.
- [122] R. Kronland-Martinet, J. Morlet, and A. Grossman, "Analysis of sound patterns through wavelet transform," *International Journal of Pattern Recognition and Artificial Intelligence*, vol. 1, pp. 237–301, 1987.
- [123] A. Paradzinets, O. Kotov, H. Harb, and L. Chen, "Continuous wavelet-like transform based music similarity features for intelligent music navigation," *2007 International Workshop on Content-Based Multimedia Indexing, Bordeaux*, pp. 165–172, 2007.
- [124] G. Tzanetakis, G. Essl, and P. Cook, "Audio analysis using the discrete wavelet transform," *Conf. Acoustics and Music: Theory 2001 and Applications (AMTA 2001)*, 2001.
- [125] A. Paradzinets, H. Harb, and L. Chen, "Use of continuous wavelet-like transform in automated music transcription," *14th European Signal Processing Conference, Florence*, 2006.